Chemie der Erde 78 (2018) 299–313

Contents lists available at ScienceDirect

Chemie der Erde

journal homepage: www.elsevier.com/locate/chemer

U–Pb geochronology, Sr–Nd isotopic compositions, geochemistry and petrogenesis of Shah Soltan Ali granitoids, Birjand, Eastern Iran

Samaneh Nadermezerji[a], Mohammad Hassan Karimpour[b,*], Azadeh Malekzadeh Shafaroudi[b], José Francisco Santos[c], Ryan Mathur[d], Sara Ribeiro[c]

[a] Department of Geology, Faculty of Science, Ferdowsi University of Mashhad, Box No. 91775-1436, Mashhad, Iran
[b] Research Center for Ore Deposit of Eastern Iran, Ferdowsi University of Mashhad, Box No. 91775-1436, Mashhad, Iran
[c] Department of Geosciences, Geobiotec Research Unit, University of Aveiro, 3810-193, Aveiro, Portugal
[d] Department of Geology, Juniata College, Huntington, PA, USA

ARTICLE INFO

Handling Editor: Hadi Shafaii Moghadam

Keywords:
Granitoids
U–Pb geochronology
Subduction
Mantle wedge
Shah Soltan Ali
Lut Block

ABSTRACT

The Shah Soltan Ali area (SSA) is located in the eastern part of the Lut Block metallogenic province. In this area different types of sub-volcanic intrusions including diorite porphyry, monzonite porphyry and monzodiorite porphyry have intruded into basaltic and andesitic rocks. Zircon U–Pb dating and field observations indicate that intermediate to mafic volcanic rocks (38.9 Ma) are older than subvolcanic units (38.3 Ma). The subvolcanic intrusions show high-K calc-alkaline to shoshonitic affinity and are metaluminous. Based on mineralogy, high values of magnetic susceptibility [(634 to 3208) $\times 10^{-5}$ SI], and low initial $^{87}Sr/^{86}Sr$ ratios, they are classified as belonging to the magnetite-series of oxidant I-type granitoids and are characterized by an enrichment in LREEs relative to HREEs, with negative Nb, Ti, Zr and Eu anomalies. These granitoids are related to volcanic arc (VAG) and were generated in an active continental margin. Low initial $^{87}Sr/^{86}Sr$ ratios (0.7043 to 0.7052) and positive εNd values (+1.48 to +3.82) indicate that the parental magma was derived from mantle wedge. Parental magma was probably formed by low degree of partial melting and metasomatized by slab derived fluids. Then assimilation and fractional crystallization processes (AFC) produced the SSA rocks. This magma during the ascent was contaminated with the crustal material.

All data suggest that Middle-Late Eocene epoch magmatism in the SSA area, occurred during subduction of Neo-Tethys Ocean in east of Iran (between Afghan and Lut Blocks).

1. Introduction

Lut Block is located in the eastern part of Iran. There are no data available on Precambrian history of Lut because no definite Precambrian outcrops have yet been found in this area (Berberian, 1977) but it exhibits a platform character in its sedimentation during the Paleozoic (Tarkian et al., 1983). The first important tectonic event in the Lut Block is related to Early Cimmerian orogeny - post Middle Triassic. During Early Cimmerian orogenic phase, the Paleozoic and lower Triassic rocks of the Central Lut were metamorphosed (Berberian, 1977). After that, Late Cimmerian orogeny occurred in Upper Jurassic-Lower Cretaceous. This orogenic phase was accompanied with metamorphism and magmatism. At that time, magmatic activity in the Lut Block began in the middle Jurassic (165-162 Ma), so that Shah Kuh and Sorkh Kuh granitoids were emplaced within metamorphic rocks (Karimpour et al., 2011). A large part of magmatism in the Lut Block is related to the subduction of Sistan Ocean which is located between the Lut and Afghan continental Blocks. This Peak of magmatism occurred in Tertiary but closure time of the Neo-Tethys Ocean is not well-defined. Some researchers consider that the collision of Lut-Afghan to have occurred at Middle Eocene (Camp and Griffis, 1982; Tirrul et al., 1983) while others have suggested that the collision occurred at Late Cretaceous (Angiboust et al., 2013; Zarrinkoub et al., 2012; Pang et al., 2013). Subduction and then extensive magmatic activities during Tertiary led to different types of mineralization. Some believe that the subduction occurred during different times (Karimpour et al., 2011); however, its mechanism is not well understood but investigation on the SSA rocks as part of the Lut Blocks can help solve this confusion. In the study area, various phases of subvolcanic bodies have emplaced during the Eocene-Oligocene. A detailed study on the SSA intrusions and

* Corresponding author.
E-mail addresses: Sa.nadermezerji@stu.um.ac.ir (N. Samaneh), karimpur@um.ac.ir (M.H. Karimpour), Shafaroudi@um.ac.ir (A. Malekzadeh Shafaroudi), jfsantos@ua.pt (J. Francisco Santos), mathur@juniata.edu (R. Mathur), sararibeiro@ua.pt (S. Ribeiro).

https://doi.org/10.1016/j.chemer.2018.08.003
Received 3 April 2018; Received in revised form 7 July 2018; Accepted 6 August 2018

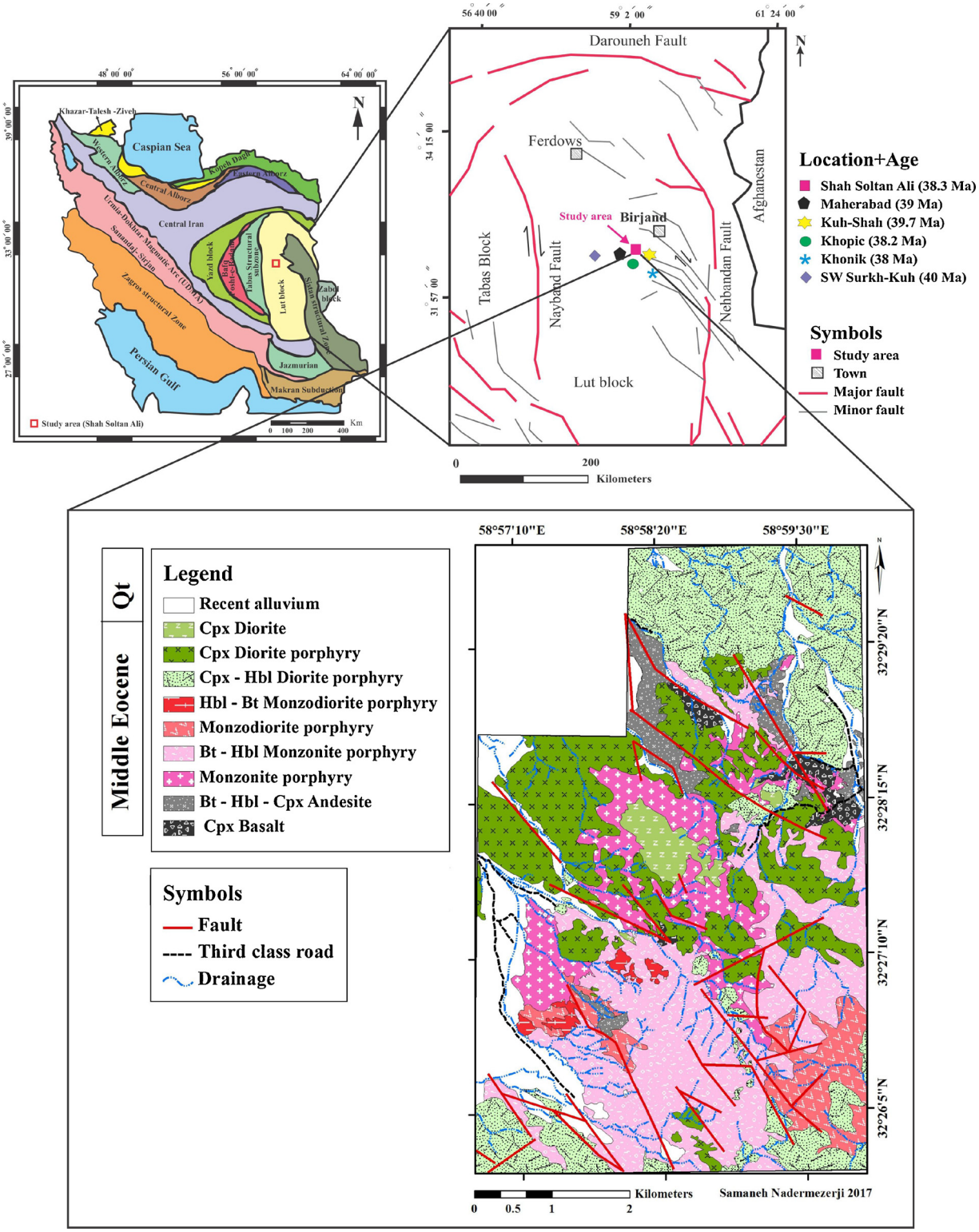

Fig. 1. Map showing location, age of intrusive rocks related to porphyry copper and epithermal deposits in the vicinity of SSA area (Summarized after Karimpour et al., 2011) the geological map of the SSA area is at the bottom (Scale 1:20,000). Hbl= Hornblende, Cpx = Clinopyroxene, Bt = Biotite (Whitney and Evans, 2010).

comparison with neighboring intrusions provides a great opportunity to shows tectonomagmatic evolution of Lut Bolck in during Eocene. Also in this regard, other enthusiasts can use geochemical data to separate the fertile intrusions from barren. In this study, the SSA geological map is prepared and the geochemical nature of subvolcanic intrusions is investigated for the first time. Finally, U-Pb dating results and Sr–Nd isotopic data are presented. All data are eventually used to investigate petrogenesis, source magma and geodynamic evolutions.

2. Geological setting and field relations

2.1. Regional geology

Lut Block extends for about 900 km in a north–south direction. It is

bounded in the north by Doruneh fault and in the south by Makran arc and Bazman volcanic complex. In the east, it is separated from Flysch Zone by the Nehbandan fault, whereas the western boundary with Central Iran is Nayband fault and Shotori Mountains (Stocklin and Nabavi, 1973) (Fig. 1).

Meso-Cenozoic magmatism in the eastern Iran is related to subduction of Neotethys oceanic crust beneath the Lut Block. Different theories have been proposed about direction of subduction and magma formation, including eastward subduction beneath the Afghan Block (Camp and Griffis, 1982; Tirrul et al., 1983), western subduction beneath the Lut Block (Zarrinkoub et al., 2012), simultaneous eastward and westward subduction (Arjmandzadeh et al., 2011), eastward intra-oceanic subduction (Saccani et al., 2010), and lithospheric removal and asthenospheric upwelling associated with extensional collapse of the east Iranian ranges (Pang et al., 2013). Also Mohammadi et al. (2016) stated that Eocene and Oligocene deformational and thermal events in the Sistan zone were controlled by late and post-collisional delamination of mantle lithosphere beneath central Iran, consistent with earlier subduction beneath the Afghan Block. It should be noted that the geological units that constitute the Lut Block testify for a complex tectonic history related to the evolution of the Sistan Ocean. Mohammadi et al. (2016) mentioned that the Sistan oceanic domain was closed during the Middle Eocene and in the next step granitic rocks were composed.

The oldest magmatic activities in the Lut Block are related to the Sorkh-Kuh, Kalateh Ahani and Shah-Kuh granitoids. These granitoids were formed during Middle Jurassic (162–171 Ma) (Tarkian et al., 1983; Moradi et al., 2011; Esmaeily et al., 2005). After that Bajestan granodiorite from Late Cretaceous (77 Ma) was emplaced within Jurassic sediments (Jung et al., 1983; Karimpour et al., 2011). The next episode of magmatism in Lut Block happened during the Tertiary. Tertiary magmatism in the Lut Block including a wide range from volcanic and plutonic rocks (Jung et al., 1983; Saadat and stern, 2016), that ignimbrites of Vaghi and Junchi, are the oldest units and after that volcanic rock types formed during middle Eocene (43–39 Ma) (Karimpour et al., 2011). Tertiary volcanic rocks are intruded by a series of subvolcanic intermediate intrusive rocks (Karimpour et al., 2009). The zircon U-Pb dating results on the subvolcanic intrusions indicate that they belong to Middle Eocene to Early Oligocene. Neogene/Quaternary volcanic activity in the Lut Block is mainly mafic in composition and located along the margins of the Lut Block (Saadat et al., 2010; Saadat and Stern, 2014) in other words from the Late Miocene to Quaternary, magmatic activity appeared to be less extensive compared to the Paleogene with various magma types, including ultrapotassic (Ahmadzadeh et al., 2010; Pang et al., 2013), adakitic (Jahangiri, 2007; Omrani et al., 2008), and alkali basaltic magmas (Allen et al., 2013; Kheirkhah et al., 2009; Pang et al., 2012; Walker et al., 2009).

2.2. Local geology

The SSA area is located in the south of geological map of Birjand (1:250,000 scale) (Vahdati Daneshmand, 1991) and northeast of the geological map of the Sar-E-Chah-E-Shur at 1:100,000 scale (Vassigh and Soheili, 1975). A large part of the Sar-E-Chah-E-Shur geological map (Vassigh and Soheili, 1975) is covered by old and young alluvial deposits. The oldest rocks detected within it are related to Upper Cretaceous Oolitic limestone and colored mélange units (Vassigh and Soheili, 1975). These units were found mainly in the central and southern parts. The Paleogene time began with limestone and conglomerate. Then andesitic and dacitic magmas were erupted during Eocene to Oligocene. Based on geological map of the Sar-E-Chah-E-Shur, magmatism in Neogene/Quaternary times was mainly andesitic to basaltic and major part of the study area is covered by intermediate to felsic lavas consisting of andesite, dacite and pyroclastic rocks as well as quaternary sediments. In the SSA area, crosscutting relationships observed in outcrops and the relationship between geological units indicate that the igneous rocks belong to three periods. The early magmatic activity is characterized by the occurrence of basaltic and andesitic eruptions. After that, monzonite porphyry and monzodiorite porphyry stocks were formed in southern parts. Finally dioritic units intruded into basic rocks and intermediate subvolcanic units including monzonite porphyry and monzodiorite porphyry. Field observations in the SSA area showed that local faults have approximately NW-SE trends and hydrothermal alteration can be related to the activity of faults. Quartz-sericite-pyrite alteration (QSP) is well developed in center and southern parts of the SSA area. The emplacement ages of mineralized subvolcanic intrusions in Maherabad (Malekzadeh Shafaroudi et al., 2010) and Kuh-Shah (Abdi and Karimpour, 2013) which are located in the vicinity of SSA area, are 39 and 39.6 Ma, respectively. These subvolcanic intrusions have characteristics similar to the SSA intrusive rocks. In the Lut Block, due to the close relationship of Cu mineralization with Eocene-Oligocene intrusive rocks, an investigation on them is very important.

3. Rock types and petrography

According to petrographic studies and zircon U-Pb dating results, geological units in the SSA area can be divided into two time windows: 1. volcanic rocks and intermediate subvolcanic intrusions related to the Middle-Late Eocene. 2. Late Eocene intermediate plutonic units with dioritic compositions.

The oldest rocks detected in the SSA area are basaltic and andesitic units. These rocks were found at the center and north of the study area (Fig. 2a). About ten subvolcanic units based on the type and abundance of phenocrysts, groundmass and mafic minerals were identified in the SSA area that all of them were categorized in three main groups: 1. Monzodiorite porphyry. 2. Monzonite porphyry. 3. Diorite porphyry (Fig. 1). Based on relative age and temporally relationships, monzodiorite porphyry units may be slightly older than monzonite porphyry units. These units intruded by diorite porphyry and indicate that the diorite porphyries are slightly younger than other unit. The subvolcanic intrusive rocks of SSA area generally have porphyritic texture with a range of fine to medium-grained groundmass.

3.1. Basalt

Basalts are the oldest volcanic rocks detected in the central and northern parts of SSA area (Fig. 1). The basaltic rocks are dark and display porphyritic, glomerporphyryitic and amygdaloidal textures with fine-grained groundmass (Fig. 2b). Their phenocrysts are mainly composed of 3–5% olivine (0.5–1 mm), 15–20% pyroxene (0.5–4 mm) and 10–12% fine plagioclase (0.3–0.6 mm). The groundmass includes plagioclase and pyroxene with minor glass. In this unit, plagioclase crystals change in composition from andesine (An30-An50) to labradorite (An50-An70). These units show propylitic alteration and secondary minerals are chlorite, epidote and carbonate.

3.2. Andesite

This group of rocks crop out in the northern and central parts of SSA area (Fig. 1). They have porphyry to glomeroporphyry texture. Their phenocrysts predominantly zoned and including 25–30% plagioclase (0.5–2 mm), 10–15% clinopyroxene (0.3–2.5 mm), 5–10% hornblende (0.3–1 mm) and 2–3% biotite (0.3–0.5 mm). Diopside is rare in phenocrysts and most of the pyroxene crystals are augite. The plagioclase phenocrysts are subhedral to euhedral, and are locally altered to epidote, calcite, and sericite. Composition of plagioclase is mainly of andesine (An30-An50). The same minerals are also present in the groundmass. Apatite is the accessory mineral (Fig. 2c) and andesitic rocks show propylitic alteration.

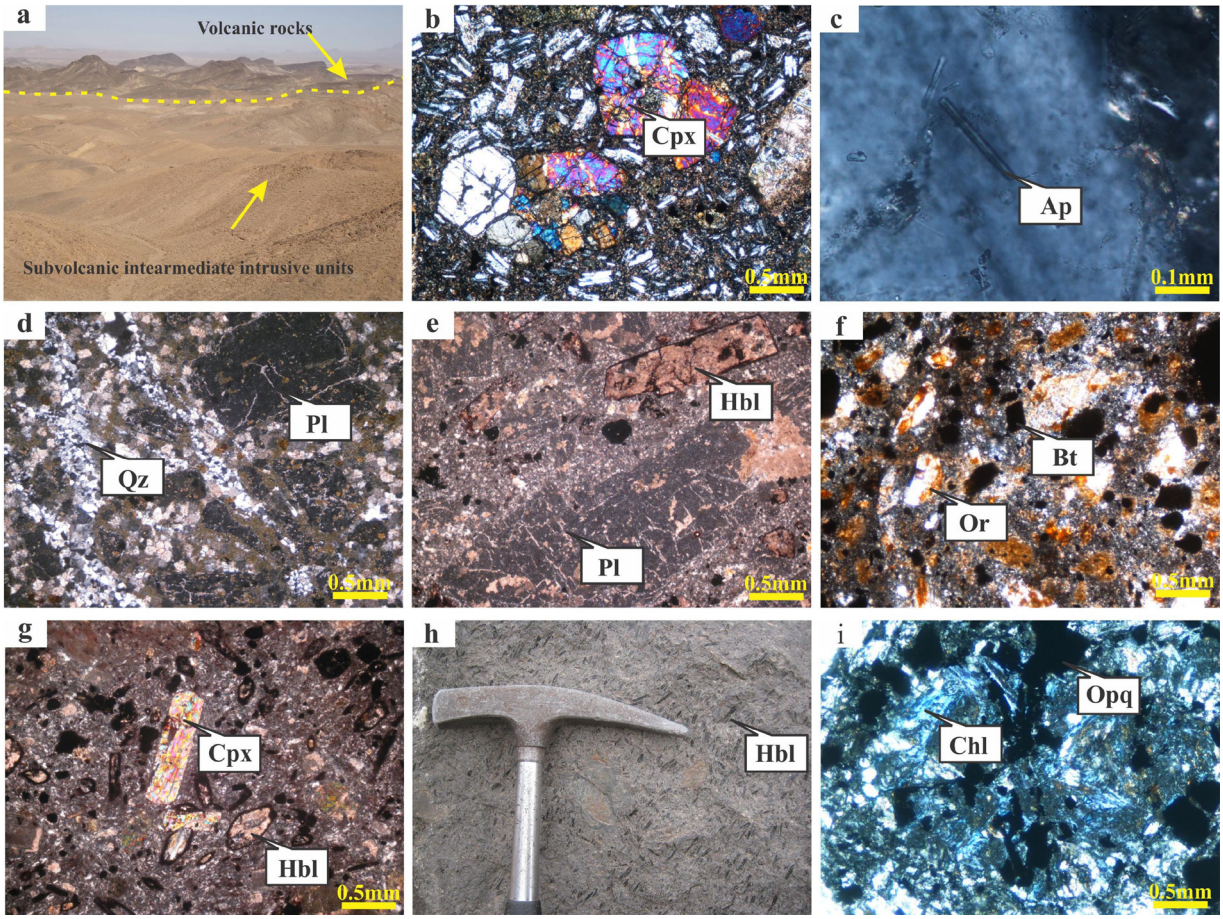

Fig. 2. Outcrops of subvolcanic and volcanic units in the SSA area (a). Clinopyroxene (augite) with glomerporphyritic texture in basaltic unite (b). Photomicrograph of apatite as the accessory mineral in andesitic unit (c). Photomicrograph of monzodiorite porphyry (d). Microscopic cross polarized light (XPL) images of hornblende biotite monzodiorite porphyry (e). Monzonite porphyry; the main minerals are plagioclase as subhedral crystals and orthoclase (f). Pyroxene hornblende diorite porphyry with porphyritic texture (g). Field photograph of pyroxene hornblende diorite porphyry (h). Photomicrograph of chlorite and opaque minerals in propylitic alteration (i). (Pl = Plagioclase, Cpx = Clinopyroxene, Hbl= Hornblende, Chl = Chlorite, Opq = Opaque, Or = Orthoclase, Qz = Quartz) (Whitney and Evans, 2010).

3.3. Monzodiorite porphyry

Monzodiorite porphyries are main stocks in the SSA area. Two types of monzodioritic phases can be distinguished based on presence and abundance of mafic minerals, such as 1. Monzodiorite porphyry (Fig. 2d), 2. Hornblende biotite monzodiorite porphyry (Fig. 2e). These units were observed in the southeast and center of the study area and they have porphyritic texture. Their phenocrysts include 20% plagioclase (1–4 mm), 5–7% K-feldspar (0.5–1.5 mm), 4–5% hornblende (0.5-0.7 mm) and 5–8% biotite (0.3-0.5 mm). The plagioclase in the monzodiorite porphyries occurs oligoclase (An10-An30) to andesine (An30-An50). Accessory minerals are apatite and zircon. Main minerals are extensively altered to sericite, quartz, calcite and clay minerals.

3.4. Monzonite porphyry

Monzonitic porphyries are shown on the south and center of the map (Fig. 1). They display porphyritic texture and due to QSP alteration, their color is dominantly yellow to cream. Monzonitic porphyries are divided into two subgroups; consisted of 1. Monzonite porphyry (Fig. 2f), 2. Biotite hornblende monzonite porphyry. Phenocrysts mainly consist of 15–17% plagioclase (1–2 mm), 8–12% K-feldspar (0.5–1 mm), 5–8% hornblende (0.3–1 mm) and 5–6% biotite (0.3-0.7 mm) in a groundmass of fine-grained plagioclase with K-feldspar. The main compositions of plagioclase phenocrysts are the range of oligoclase (An10-An30) to andesine (An30-An50). Zircon is common an accessory mineral and phenocrysts are altered to sericite, calcite, quartz and clay minerals.

3.5. Diorite porphyry

Dioritic porphyries are the youngest subvolcanic rocks in the north and center of SSA area (Fig. 1). These units exhibit the variety of porphyry to glomeroporphyry texture. Based on the type and abundance of mafic minerals, about two dioritic units are identified, such as pyroxene hornblende diorite porphyry (Fig. 2g, h) and pyroxene diorite porphyry. Diorite porphyry phenocrysts are composed of 20–25% euhedral plagioclase (0.5–2.5 mm), 8–10% pyroxene (0.5–1.5 mm), 5–7% hornblende (0.3–1 mm) and 3–5% biotite (0.3-0.7 mm). Pyroxene crystals are commonly augite and the diopside type is less common. Plagioclase varies from oligoclase (An10-An30) to andesine (An30-An50). Apatite and zircon occur as accessory minerals in the diorite porphyry. It is greenish gray in color, and has intermediate propylitic alteration (Fig. 2i).

4. Material and methods

More than 200 thin sections were prepared from all rock samples collected from surface. Ten samples were selected for chemical analyses. Almost all selected samples were unaltered. These ten samples

were analyzed for major elements by wavelength-dispersive X-ray Fluorescence (XRF) spectrometry using fused discs and the Phillips PW 1480 XRF at the East Amethyst Laboratory in Mashhad, Iran. Nine of samples were analyzed by the ICP-MS method for minor and trace elements using lithium metaborate/tetraborate fusion and nitric acid total digestion, in the ACME Laboratories, Vancouver, Canada. Sr and Nd isotopic compositions were determined for five samples at Laboratório de Geologia Isotópica da Universidade de Aveiro, Portugal. The $^{87}Sr/^{86}Sr$ and $^{143}Nd/^{144}Nd$ isotopic ratios were determined using a multi-collector Thermal Ionization Mass Spectrometer (TIMS) VG Sector 54. Data were acquired in dynamic mode with peak measurements at 1–2 V for ^{88}Sr and 0.5–1.0 V for ^{144}Nd. The Nd and Sr natural isotopic ratios were normalized for mass fractionation relative to $^{88}Sr/^{86}Sr = 0.1194$ and $^{146}Nd/^{144}Nd = 0.7219$. During this study, average and 1ϕ for isotope ratio standards into the SRM-987 and JNdi-1 are $^{87}Sr/^{86}Sr = 0.710268 \pm 13$ (N = 5; conf. lim = 95%, 2 r) and $^{143}Nd/^{144}Nd = 0.5120985 \pm 53$ (N = 5; conf. lim = 95%), respectively. For Rb and Sm isotopic compositions, the values recommended by IUPAC (Berglund and Wieser, 2011) were used. The CHUR (Chondritic Uniform Reservior) values, $^{147}Sm/^{144}Nd = 0.1967$ and $^{143}Nd/^{144}Nd = 0.512638$ were used to calculate the ε° (DePaolo and Wasserburg, 1976). Two samples of subvolcanic and volcanic units, each one 10–15 kg, were collected for U–Pb dating of zircon. Approximately 61 zircon grains were hand-picked from each sample under a binocular microscope and then Zircons were dated using the Laser Ablation (LA)-ICP-MS method at Washington State University. CL imaging (University of Idaho) using a New Wave Nd: YAG UV 213-nm laser coupled to a Thermo Finnigan Element 2 single collector, double-focusing, magnetic sector ICP-MS. Operating procedures and parameters are a modifications of Chang et al. (2006). Results of the ICP-MS analyses were evaluated using GCDKIT software version 3 and data processing and geological mapping was done by Arc GIS software version 10.

5. Geochemistry of the intrusive rocks

5.1. Major elements

Plagioclase and K-feldspar minerals are the main components of the SSA subvolcanic intrusions. In the monzodiorite porphyry units, plagioclase is the dominant mineral and constitutes about 60%–75% of the rock volume whereas K-feldspar is relatively low. K-feldspar and plagioclase are main minerals in monzonitic porphyries and their modal abundance varies from 20% to 25 and 50%, respectively. The diorite porphyry is composed mainly of plagioclase which is observed both as large phenocrysts and as small grains in the groundmass. Biotite, hornblend and clinopyroxene are the major ferromagnesian minerals. In this section, subvolcanic units will be classified based on the whole chemical composition of the rock (bulk compositions).

Major elements data of the SSA subvolcanic units are presented in Table 1. The SSA subvolcanic rocks show a limited range of SiO_2 from 53.12 to 59.79 wt. %, while the total alkalis ($Na_2O + K_2O$) range from 5.58 to 7.35 wt. % (Table 1). Based on TAS diagram of Middlemost (1985) (Fig. 3a), these samples plot in the field of diorite, monzodiorite and monzonite. These results of geochemical classification are confirmed by petrographic studies. The K_2O content of these units was between 3.00 wt. % and 4.00 wt. % (Table 1). A plot of K_2O vs. SiO_2 wt. % (Peccerillo and Taylor, 1976) shows that the subvolcanic rocks fall in the field of high-K calk-alkaline to shoshonite series (Fig. 3b). A/CNK ratios mostly ranged from 0.66 to 0.87 and A/NK values show a range of 1.47–2.06, consistent with metaluminous compositions (Shand, 1949) (Fig. 3c).

5.2. Trace elements

Trace and REE element compositions of the analyzed samples in the SSA area are illustrated in Table 1. Primitive mantle-normalized trace element spider diagrams (Sun and McDonough, 1989), show enrichment in light rare earth elements (LREEs) and large ion lithophile elements (LILEs; e.g., Rb, Cs, K, and Sr), against depletion in HREEs and high field strength elements (HFSEs; e.g., Nb, Zr, and Ti) (Fig. 4a). These depletion and enrichment of elements are characteristics of magmas formed in subduction zones (Wilson, 1989).

The chondrite-normalized REE patterns (Boynton, 1984) (Fig. 4b) of the subvolcanic units are uniform, similar and parallel. They exhibit a fairly steep slope of light rare earth elements against heavy rare earth elements (LREE/HREE) and flat patterns of HREE are shown by ratios of $(Dy/Yb)_N$ that vary from 1.03 to 1. The parallel trend of chondrite-normalized (Boynton, 1984) REEs pattern in intermediate subvolcanic rocks can be explained by similarity of the magmatic processes during the formation (Richards, 2012) also moderate enrichment of light REE (LREE) is confirmed by $(La/Sm)_N = 2.49–3.67$. All of the subvolcanic intrusive rocks display low La_N/Yb_N (4.6–9.7) and Ce_N/Yb_N (3.17–7) ratios as well as a negative Eu anomaly.

6. Magnetic susceptibility

The granitoids were divided into the magnetite series and the ilmenite series by Ishihara (1977). According to Ishihara (1977), magnetic susceptibility value of magnetite series is about $> 50.0 \times 10^{-5}$ (SI) (Ishihara, 1981) whereas Magnetic susceptibility of the SSA subvolcanic intrusions is more than 634×10^{-5} (SI) (631×10^{-5} to 3208 631×10^{-5} SI). Based on mineralogy and high values of magnetic susceptibility, SSA subvolcanic units are classified as belonging to the magnetite-series of oxidant I-type granitoids (Fig. 3d).

7. U-Pb zircon age dating

Among the SSA igneous rocks, two representative samples were chosen from volcanic rocks (N118; Andesite) and subvolcanic intrusions (N164; monzodiorite porphyry) for zircon U-Pb dating (Table 2). Approximately 61 zircon grains were separated from the andesite sample and 33 points were selected for the analysis of the margin and the center of zircon grains. In this sample, zircon grains are yellow, anhedral to subhedral and they are between 50 and 250 μm long (Fig. 5a). According to zircon U-Pb dating, mean age of andesite unit is 38.9 ± 0.6 Ma (Fig. 6a, b). Mineralized monzodiorite porphyry (host rock) was selected for dating. The zircon grains of monzodiorite porphyry were transparent, white to yellow, 50–280 μm in length, euhedral to subhedral and showed oscillatory zoning in Cl images (Fig. 5b), which suggested a magmatic origin. Nearly 72 zircon grains were isolated and based on 31 analyzed points; the mean age was estimated to be 38.3 ± 0.5 Ma for monzodiorite porphyry unit (Fig. 6c, d). These results indicate that the oldest units in the SSA area are volcanic rocks. These characteristics with the high closure temperatures of zircon (Cherniak and Watson, 2000) allowed us to interpret the U–Pb data as representative of the crystallization age of the respective igneous rocks indicating that the intrusion occurred in the Middle-Late Eocene (Bartonian).

Field observations indicated that volcanic rocks have a sharp contact with subvolcanic intrusions and these volcanic rocks were cut by dioritic, monzodioritic and monzonic phorphyries. In the vicinity of these contacts, the size of minerals decreased. In fact decreasing the grains size depends solely on the cooling rate. Based on field observations and U-Pb dating results, volcanic rocks are slightly older than subvolcanic phorphyries.

8. Sr-Nd isotopic ratios

Based on petrographic studies, five least altered samples from the SSA subvolcanic units were selected for Sr–Nd isotopic analysis the analytical data of which is summarized in Table 3a and b. Initial

Table 1
Major (wt. %) and trace elements (ppm) analysis of the SSA intrusive rocks.

Sample No.	N18	N19	N24	N46	N47	N98	N102	N122	N128	N138
X	32°29′14″	32°29′14″	32°25′48″	32°27′38″	32°27′07″	32°28′11″	32°28′03″	32°28′07″	32°27′46″	32°28′48″
Y	58°59′23″	58°59′24″	58°58′10″	58°58′54″	58°58′38″	58°59′50″	58°59′35″	58°59′18″	58°58′54″	58°59′17″
Rock type	3	1	3	2	1	1	1	3	1	3
SiO_2	58.92	59.79	58.22	59.6	57.88	53.62	54.05	55.47	53.12	55.42
TiO_2	0.6	0.64	0.63	0.52	0.65	0.73	0.72	0.73	0.74	0.73
Al_2O_3	15.66	16.25	15.23	15.2	15.52	15.04	15.29	15.53	14.56	15.49
TFeO	6.38	5.7	6.04	5.6	6.23	8.38	8.37	8.5	8.33	7.51
MnO	0.11	0.11	0.1	0.12	0.1	0.13	0.12	0.13	0.17	0.13
MgO	3.99	1.21	2.99	2.1	3.82	5.86	5.35	5.62	7.08	4.69
CaO	5.5	6.48	5.49	4.7	5.35	7.29	6.79	7	6.65	6.97
Na_2O	2.92	3.35	3.09	3.4	3.04	2.86	2.49	2.65	2.63	2.7
K_2O	3.09	4	3.86	3.8	3.09	3.77	3.09	3.42	3.35	3
P_2O_5	0.27	0.45	0.31	0.3	0.34	0.27	0.3	0.3	0.28	0.43
L.O.I	2.35	2.01	3.8	4.2	2.87	2.32	2.1	1.47	2.83	2.61
Total	99.79	99.9	99.76	99.54	98.89	100.26	98.67	100.42	99.74	99.68
Ba	792	696	749	–	1086	792	573	585	679	571
Cs	2.9	4.9	6.6	–	3.2	1	2.7	1.2	3.6	0.4
Hf	2.6	2.7	2.5	–	3.1	1.5	1.8	2	1.8	2.2
Nb	4.4	4.8	4.5	–	5..4	2	1.9	1.9	2	2
Rb	74.5	92.3	94.1	–	102.2	54.2	62.1	64.9	74.6	53.3
Sr	887.2	959.6	840.6	–	894.4	627.7	628.7	640.1	949.1	774.9
Ta	0.3	0.3	0.4	–	0.4	0.1	0.1	0.1	0.1	0.1
Zr	98.1	102.6	94.2	–	109.6	57.3	61.9	59.7	59.4	68.1
Y	32	16	37	–	37	24	31	26	32	30
La	23.6	26.1	24.9	–	25.1	14.1	15.5	14.5	15.3	18
Ce	62.4	49.5	44.7	–	49.2	26.9	28.1	26	29	34.6
Pr	5.23	5.96	5.43	–	5.9	3.55	3.78	3.83	3.8	4.85
Nd	22	25.6	21.3	–	24	17	16.5	17.3	16	21.9
Sm	4.7	4.85	4.27	–	4.88	3.51	3.76	3.61	3.61	4.54
Eu	1.17	1.3	1.24	–	1.23	0.95	1.05	1.02	0.96	1.26
Gd	4.11	4.14	3.84	–	4.26	3.45	3.61	3.76	3.52	4.06
Tb	0.56	0.55	0.55	–	0.59	0.5	0.55	0.54	0.54	0.61
Dy	3.23	3.14	3.17	–	3.39	3.16	3.47	3.45	3.06	3.5
Ho	0.75	0.62	0.64	–	0.6	0.63	0.61	0.69	0.62	0.75
Er	2.22	1.64	1.89	–	1.98	1.75	2.05	2.08	1.84	2.24
Tm	0.29	0.27	0.28	–	0.29	0.27	0.3	0.31	0.29	0.33
Yb	2.09	1.81	1.82	–	1.89	1.84	1.96	2.12	1.91	2.08
Lu	0.35	0.27	0.25	–	0.3	0.31	0.32	0.3	0.29	0.35
Ratios										
Eu/Eu*	0.81	0.89	0.94	–	0.82	0.87	0.83	0.85	0.82	0.90
$(La/Yb)_N$	7.61	9.72	9.22	–	8.95	5.17	5.33	4.61	5.40	5.83

$^{87}Sr/^{86}Sr$ ratios and εNd(i) values were calculated according to the crystallization age of monzodiorite porphyry unit (t = 38.3 Ma). The initial $^{87}Sr/^{86}Sr$ and εNd (i) of dioritic and monzodioritic intrusions vary in a limited range from 0.7043 to 0.7052 and from +1.48 to +3.81 respectively. Initial $^{87}Sr/^{86}Sr$ ratios obtained from N18 and N128 samples were slightly higher than other samples. This means that the magma did not originate from continental crust. In the εNd(i) vs. ($^{87}Sr/^{86}Sr$)i diagram (Fig. 7), all samples plot to the right of the so-called mantle array and overlaps the field of island-arc basalts (IAB).

Most of magmatic activity in the Lut Block occurred in middle Eocene (Karimpour et al., 2011), and all of the granitoid rocks formed in the vicinity of SSA area belong to Middle-Late Eocene. Maherabad and Khopik (39 Ma), Kuh-Shah (39.6 Ma), Khunik (38) and Sorkh-Kuh (40 Ma) intrusive rocks are metaluminous and the REE spider patterns of them are similar to the signatures seen in island arc intrusive rocks. These granitoids have high values of magnetic susceptibility [(84 to 7627) × 10^{-5} SI]. The initial $^{87}Sr/^{86}Sr$ ratios and εNd (i) isotope values for the Maherabad and Khopik, Khunik, Kuh-Shah and SW Sorkh-Kuh intrusive rocks are reported in Table 4. Their initial $^{87}Sr/^{86}Sr$ and εNd (i) ratios range from 0.704196 to 0.706692 and from -0.18 to +3.3, respectively. Therefore the magma did not originate from the continental crust and almost all of them formed in volcanic arc setting related to subduction zone.

This suggests that magma in Lut Block originated from mantle above a subduction zone and the mantle source is affected by subduction-related fluids and/or sediments. The recorded small variation in isotopic ratios can be related to variable crustal assimilation, hydrothermal alteration or heterogeneity in the magma source (Nabatian et al., 2014).

9. Discussion

9.1. Magma petrogenesis and source characteristics

Calc-alkaline rocks typically are found in the arcs above subduction zones and calc-alkaline series are divided to High-K, Med-K and Low-K (Sheth et al., 2002). Previous studies showed that SSA granitoids have high-K calc-alkaline affinity and belong to I-type series. They show enrichment of LILE compared to HFSE elements. For example positive anomalies of Rb, Cs, K, and Sr elements and negative anomalies of Ti, Zr and Nb are observed in all samples. The negative anomalies of Ti and Zr can be related to the presence of Fe-Ti oxides and zircon mineral as remaining mineral phases in source (Martin, 1999; Rollinson, 1993). Negative Nb anomaly is recognized as a fingerprint of a subduction and is also characteristic of the continental crust (Nagudi et al., 2003). In many cases, negative Nb anomaly and positive anomalies of Rb, Cs, Ba and K elements are probably related to the processes of assimilation, contamination or mixing with crustal materials (Asran and Rahman, 2012; Rollinson, 1993; Wilson, 1989; Zhang et al., 2006). During subduction, released fluids of the subducted lithosphere and low degree of partial melting provide enrichment of LILE compared to HFSE elements. In the SSA intrusive rocks, the Sr/Y ratio is less than 29.65 in all

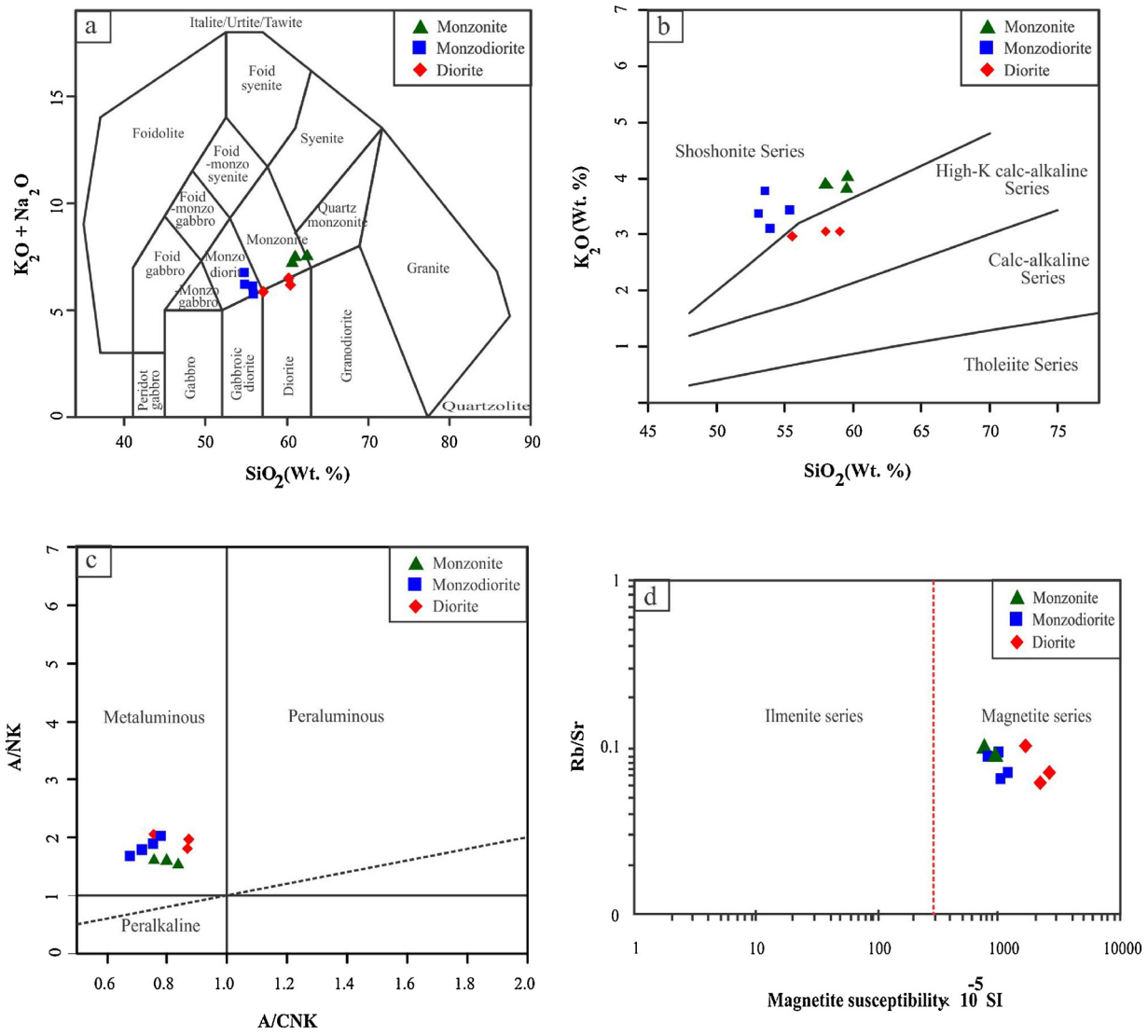

Fig. 3. Geochemical classification of the SSA intrusive rocks, according to $Na_2O + K_2O$ vs. SiO_2 diagram (Middlemost, 1985) (a). Geochemical variations in analyzed samples of the SSA area, based on K_2O vs. Si_2O diagram (Peccerillo and Taylor, 1976) (b). $Al_2O_3/Na_2O + K_2O$ (molar) vs. $Al_2O_3/$ (CaO + K_2O + Na_2O) (molar) diagram of SSA subvolcanic rocks (Shand, 1949) (c). A plot of Rb/Sr vs. magnetic susceptibility (Karimpour et al., 2011). The line divides the magnetite series field from the ilmenite series field (d).

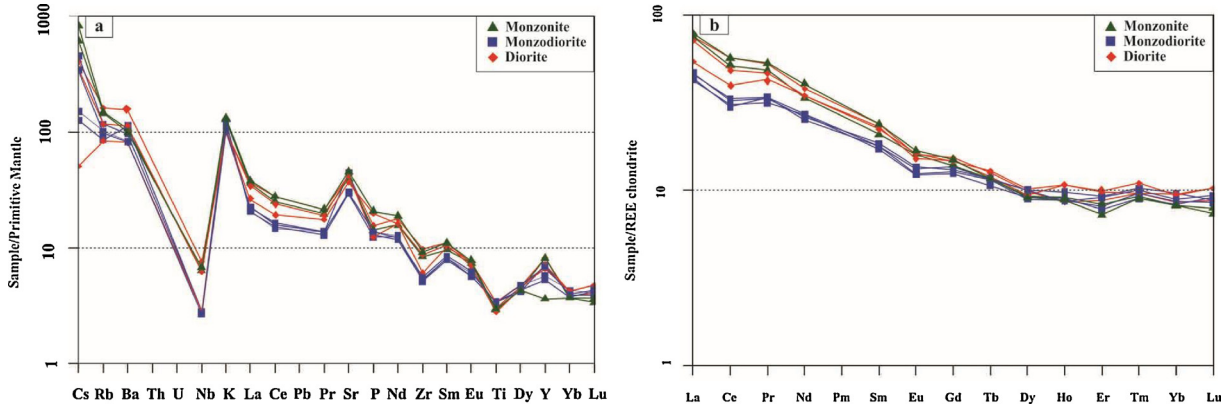

Fig. 4. Primitive mantle normalized patterns for the SSA intrusive rocks (Sun and McDonough, 1989) (a). Chondrite-normalized REE diagram for the SSA intrusive rocks (Boynton, 1984) (b).

Table 2
U–Pb dating results of zircons related to two samples of volcanic (N118) and subvolcanic units (N164).

Sample	U (ppm)	U/Th (ppm)	Pb 207 Corrected					Non Corrected				Age	
			$^{207}Pb/^{235}U$	2 s Abs Error	$^{206}Pb/^{238}U$	2 s Abs Error	Corr. Coef.	$^{238}U/^{206}Pb$	2 s Abs Error	$^{207}Pb/^{206}Pb$	2 s Abs Error	Best Age	2 s Abs Error
N 118: Andesite													
118_1	224	2.0	0.03701	0.00382	0.00583	0.00026	0.680	171.7154	7.5200	0.0461	0.0037	37.5	1.6
118_2	322	2.9	0.07665	0.00963	0.00576	0.00040	0.704	163.8462	10.8271	0.0911	0.0084	37.0	2.5
118_3	412	1.7	0.03759	0.00284	0.00616	0.00027	0.754	162.9042	7.2564	0.0444	0.0023	39.6	1.8
118_4	288	2.0	0.03998	0.00355	0.00600	0.00028	0.717	166.2857	7.7831	0.0482	0.0031	38.6	1.8
118_5	164	1.9	0.03024	0.00407	0.00605	0.00031	0.667	167.3984	8.7566	0.0367	0.0039	38.9	2.0
118_6	807	2.3	0.04033	0.00253	0.00604	0.00025	0.805	165.1268	6.8633	0.0483	0.0018	38.8	1.6
118_8	452	1.9	0.04804	0.00438	0.00609	0.00035	0.765	162.0697	9.2937	0.0565	0.0034	39.2	2.2
118_9	219	2.7	0.03719	0.00389	0.00619	0.00030	0.687	162.1339	7.7963	0.0437	0.0035	39.8	1.9
118_10	523	2.2	0.03904	0.00270	0.00629	0.00028	0.786	159.3715	7.0832	0.0451	0.0020	40.4	1.8
118_11	712	2.8	0.04920	0.00366	0.00608	0.00033	0.828	162.2175	8.7005	0.0579	0.0025	39.1	2.1
118_12	298	2.8	0.03811	0.00351	0.00594	0.00031	0.737	168.5030	8.9414	0.0466	0.0030	38.2	2.0
118_13	276	2.4	0.03851	0.00348	0.00611	0.00028	0.712	163.9973	7.6640	0.0458	0.0030	39.2	1.8
118_14	323	2.7	0.04446	0.00388	0.00593	0.00029	0.733	167.0857	8.2040	0.0539	0.0033	38.1	1.9
118_15	870	2.5	0.03851	0.00235	0.00600	0.00019	0.746	166.6670	5.3969	0.0466	0.0020	38.6	1.3
118_16	247	2.7	0.03944	0.00398	0.00614	0.00028	0.687	162.8144	7.4601	0.0466	0.0036	39.5	1.8
118_18	166	2.1	0.03905	0.00433	0.00607	0.00029	0.677	164.7245	7.7610	0.0467	0.0040	39.0	1.8
118_19	322	1.1	0.04564	0.00548	0.00595	0.00027	0.671	166.2690	7.3722	0.0551	0.0053	38.2	1.7
118_20	185	2.0	0.04375	0.00528	0.00603	0.00046	0.758	164.5934	12.5505	0.0522	0.0042	38.8	3.0
118_21	604	2.4	0.04182	0.00314	0.00574	0.00025	0.751	173.0316	7.5614	0.0525	0.0027	36.9	1.6
118_22	536	2.4	0.03908	0.00367	0.00609	0.00040	0.803	164.2856	10.7542	0.0466	0.0027	39.1	2.6
118_23	399	2.3	0.04533	0.00508	0.00631	0.00035	0.697	157.3642	8.7763	0.0518	0.0043	40.6	2.3
118_24	272	2.8	0.03787	0.00312	0.00587	0.00027	0.735	170.2518	7.8554	0.0468	0.0027	37.8	1.7
118_25	570	2.5	0.04437	0.00293	0.00614	0.00028	0.819	161.8307	7.4369	0.0521	0.0020	39.4	1.8
118_26	614	2.6	0.04001	0.00313	0.00618	0.00033	0.803	161.6955	8.6446	0.0469	0.0022	39.7	2.1
118_28	559	2.0	0.06763	0.00543	0.00931	0.00054	0.823	106.7035	6.1708	0.0524	0.0024	59.7	3.4
118_30	280	2.3	0.03761	0.00385	0.00586	0.00034	0.732	170.7788	10.0577	0.0466	0.0033	37.6	2.2
118_31	342	3.4	0.03989	0.00332	0.00612	0.00030	0.747	163.3337	7.9635	0.0473	0.0027	39.3	1.9
118_33	217	2.6	0.03325	0.00425	0.00640	0.00040	0.690	157.9315	9.8723	0.0381	0.0037	41.1	2.6
118_34	242	2.4	0.03388	0.00467	0.00574	0.00039	0.692	175.0133	12.0724	0.0430	0.0044	36.9	2.5
118_35	1163	3.0	0.03732	0.00269	0.00581	0.00028	0.794	172.1361	8.2113	0.0466	0.0021	37.3	1.8
118_36	187	2.5	0.05615	0.00570	0.00598	0.00035	0.729	162.9451	9.3605	0.0664	0.0047	38.5	2.2
118_37	454	2.2	0.03622	0.00296	0.00606	0.00032	0.786	165.7959	8.9121	0.0436	0.0022	38.9	2.1
118_38	686	2.7	0.04653	0.00335	0.00592	0.00030	0.812	166.907	8.3328	0.0563	0.0024	38.0	1.9
N164 : Monzodiorite													
164_1	313	2.1	0.08891	0.01334	0.00559	0.00040	0.673	165.1577	11.0399	0.1065	0.0124	36.0	2.5
164_2	257	1.9	0.03780	0.00375	0.00586	0.00025	0.685	170.7429	7.4318	0.0468	0.0036	37.6	1.6
164_3	304	1.8	0.03805	0.00331	0.00587	0.00027	0.718	170.2702	7.7898	0.0470	0.0030	37.7	1.7
164_4	478	1.3	0.03872	0.00285	0.00613	0.00025	0.738	163.2982	6.5989	0.0459	0.0024	39.4	1.6
164_5	430	1.9	0.03823	0.00239	0.00581	0.00023	0.788	171.8807	6.7829	0.0477	0.0019	37.4	1.5
164_6	300	2.2	0.03859	0.00363	0.00588	0.00023	0.685	169.8809	6.7548	0.0476	0.0035	37.8	1.5
164_7	742	2.7	0.03973	0.00251	0.00603	0.00022	0.759	165.7364	5.9968	0.0478	0.0020	38.7	1.4
164_8	239	2.4	0.04011	0.00357	0.00622	0.00025	0.692	160.7115	6.4073	0.0468	0.0032	40.0	1.6
164_9	520	2.2	0.07469	0.00430	0.00604	0.00023	0.797	157.4340	5.7536	0.0853	0.0031	38.8	1.4
164_10	298	2.8	0.03911	0.00305	0.00596	0.00027	0.752	167.5380	7.7083	0.0475	0.0025	38.3	1.8
164_12	262	1.8	0.03791	0.00335	0.00587	0.00026	0.711	170.2674	7.6656	0.0468	0.0030	37.7	1.7
164_13	236	2.6	0.05634	0.00509	0.00595	0.00027	0.704	163.7001	7.2921	0.0669	0.0045	38.3	1.7
164_14	462	1.7	0.03903	0.00284	0.00598	0.00024	0.742	167.1729	6.8033	0.0473	0.0024	38.4	1.6
164_15	265	2.4	0.04402	0.00399	0.00592	0.00028	0.715	167.4112	7.9309	0.0535	0.0035	38.1	1.8
164_16	291	1.8	0.03897	0.00357	0.00611	0.00027	0.700	163.6840	7.2632	0.0463	0.0032	39.3	1.7
164_17	1139	2.9	0.03863	0.00216	0.00598	0.00021	0.800	167.2102	5.9397	0.0469	0.0016	38.4	1.4
164_18	352	2.7	0.06287	0.00445	0.00606	0.00027	0.769	159.6501	6.9020	0.0728	0.0034	38.9	1.7
164_19	396	2.4	0.04592	0.00340	0.00626	0.00026	0.742	158.5145	6.5890	0.0528	0.0027	40.2	1.7
164_20	480	2.4	0.03901	0.00283	0.00578	0.00022	0.728	172.4861	6.5262	0.0488	0.0025	37.2	1.4
164_21	231	2.1	0.07006	0.00601	0.00579	0.00031	0.750	164.5448	8.4162	0.0836	0.0049	37.2	1.9
164_22	310	1.7	0.03810	0.00343	0.00600	0.00026	0.701	166.8019	7.2599	0.0461	0.0031	38.6	1.7
164_23	683	1.9	0.03774	0.00242	0.00577	0.00024	0.798	173.1524	7.2685	0.0474	0.0019	37.1	1.6
164_24	205	2.2	0.03522	0.00432	0.00592	0.00027	0.670	169.6333	7.8138	0.0433	0.0042	38.1	1.8
164_25	1407	1.2	0.05706	0.00272	0.00843	0.00031	0.893	118.3923	4.3393	0.0490	0.0011	54.1	2.0
164_26	414	2.3	0.03657	0.00277	0.00578	0.00026	0.755	173.2233	7.7696	0.0460	0.0023	37.1	1.7
164_27	270	2.3	0.05028	0.00453	0.00602	0.00027	0.702	163.2948	7.1652	0.0596	0.0040	38.7	1.7
164_28	350	1.6	0.03845	0.00338	0.00596	0.00024	0.697	167.8087	6.8438	0.0468	0.0031	38.3	1.6
164_29	220	1.9	0.05099	0.00540	0.00601	0.00025	0.676	163.6058	6.7589	0.0605	0.0051	38.6	1.6
164_30	293	1.7	0.04845	0.00466	0.00626	0.00031	0.705	157.8761	7.6684	0.0555	0.0039	40.3	2.0
164_36	240	1.5	0.04473	0.00442	0.00601	0.00031	0.604	165.0258	8.3570	0.0535	0.0043	38.6	2.0
164_41	105	1.2	0.03574	0.00549	0.00592	0.00038	0.520	169.6328	11.0406	0.0440	0.0058	38.0	2.5

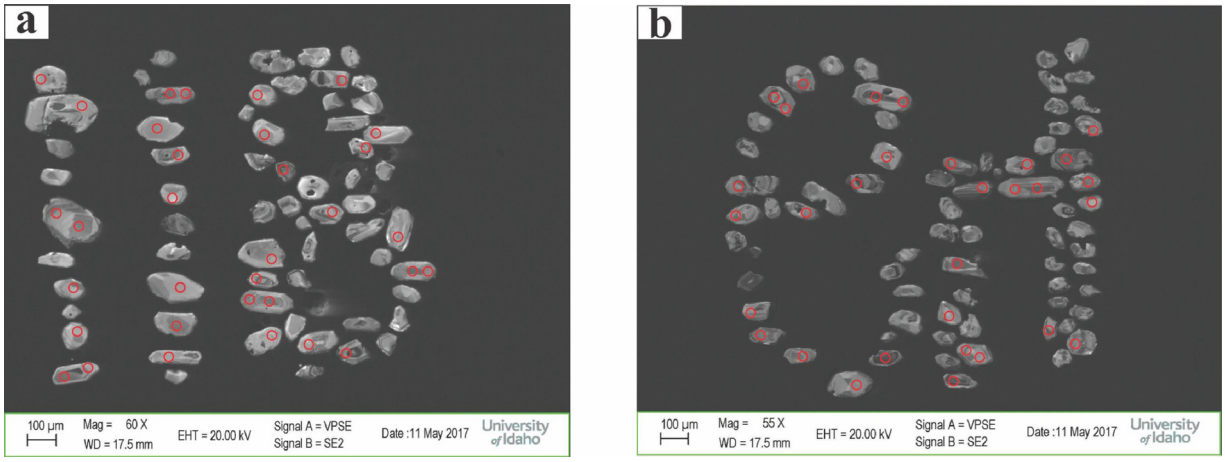

Fig. 5. Cathodo-luminescence images of representative zircon grains from andesite (N 118) (a) and monzodiorite porphyry (N 164) (b).

samples except N19 sample (Sr/Y = 58.51). Sr/Y vs. Y diagram from Defant and Drummond (1990), shows an almost linear trend within the classic island-arc field and low Sr/Y ratios (< 29.65) in subvolcanic units related to the presence of plagioclase mineral in the source magma (Fig. 8a). The $(La/Yb)_N$ and $(Ce/Yb)_N$ ratios of subvolcanic rocks vary from 4.6 to 9.7 and 3.17 to 7, respectively. These ratios suggest LREE moderate enrichment compared to HREE and the lack or the presence of a little garnet in the source of magma. Also, they show parental melts formed at a shallow depth, outside the stability field of garnet. The content of La and La/Sm ratios is about 14.1 to 26.1 and 3.96 to 5.83 respectively. According to La/Sm vs. La diagram of Blein et al, (2001) (Fig. 8b), it is clear that SSA samples follow the partial melting trend. The Th/Yb vs. Ta/Yb ratios (Pearce, 1983) can be used to define the origin of magma. According to this diagram (Fig. 9a), intrusive rocks are originated from enriched mantle and they are plotted in mantle metasomatism field. In Ba/La vs. Th/Nd diagram (Shaw, 1970), Fluids derived of subducted continental sediments can be considered as the metasomatism factor (Fig. 9b).

Present minerals in the source are shown by various diagrams. The Ce/Sm and Sm/Yb ratios (COBAN, 2007) in SSA intrusions vary from 7.20 to 10.46 and 1.70 to 2.67, respectively. These ratios indicate that there is no garnet mineral as remaining mineral phases in the source of parental magmas (Fig. 10a). According to La/Sm vs. Sm/Yb diagram (Kay and Mpodozis, 2001), clinopyroxene and amphibole were existed in source (Fig. 10b). Clinopyroxene and amphiboles are stable at a depth less than 35 km and 30 to 45 km, respectively. Due to the lack of

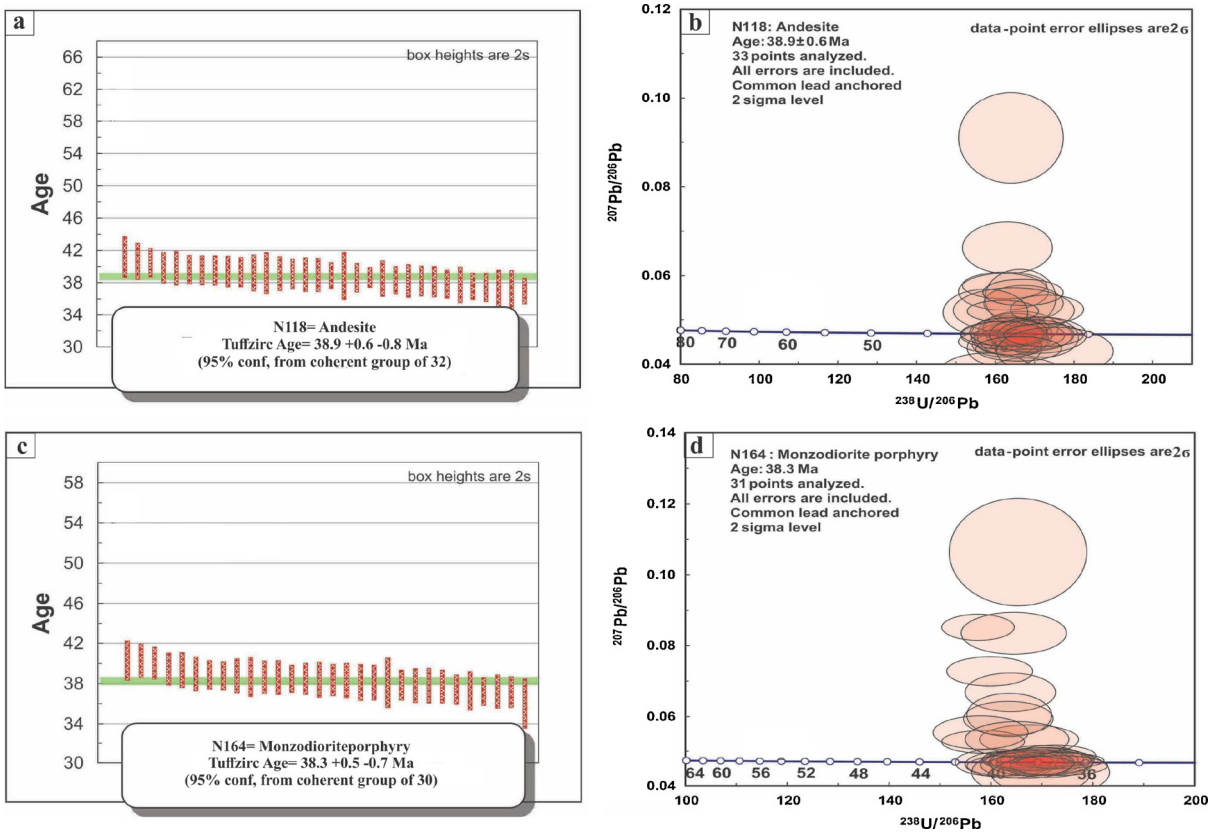

Fig. 6. TuffZirc plot illustrating zircon age for N118-andesite sample (a), Tera-Wasseburg Concordia diagrams of N118-andesite sample (b), TuffZirc plot showing zircon age for N164- monzonite porphyry sample (c), Tera-Wasseburg Concordia diagrams of N164- monzodiorite porphyry sample (d).

Table 3
a) The Rb-Sr isotopic data of five whole-rock samples from the SSA area. b) The Sm–Nd isotopic data of five whole-rock samples from the SSA area.

(a)

Rb-Sr isotopic data

Sample	Sr (ppm)	Rb (ppm)	$^{87}Rb/^{86}Sr$ sample	Error (2 s)	$^{87}Sr/^{86}Sr$ Measured	Error (2 s)	$(^{87}Sr/^{86}Sr)i$
N18	887.2	74.5	0.243	0.007	0.705418	0.000025	0.705286
N98	627.7	54.2	0.250	0.007	0.704532	0.000025	0.704396
N122	640.1	64.9	0.293	0.008	0.704516	0.000024	0.704356
N128	949.1	74.6	0.227	0.006	0.705012	0.000023	0.704888
N138	774.9	53.3	0.199	0.006	0.704561	0.000023	0.704453

(b)

Sm-Nd isotopic data

Sample	Nd (ppm)	Sm (ppm)	$^{147}Sm/^{144}Nd$ sample	Error (2 s)	$(^{143}Nd/^{144}Nd)$ measured	$(^{143}Nd/^{144}Nd)i$	Error (2 s)	(εNd)i	TDM (Ga)
N18	22.0	4.70	0.129	0.007	0.512697	0.512665	0.000012	1.48	0.95
N98	17.0	3.51	0.125	0.007	0.512796	0.512764	0.000022	3.42	0.59
N122	17.3	3.61	0.126	0.007	0.512775	0.512743	0.000019	3.01	0.59
N128	16.0	3.61	0.136	0.007	0.512818	0.512784	0.000021	3.81	0.54
N138	21.9	4.54	0.125	0.007	0.512791	0.512759	0.000012	3.32	21.47

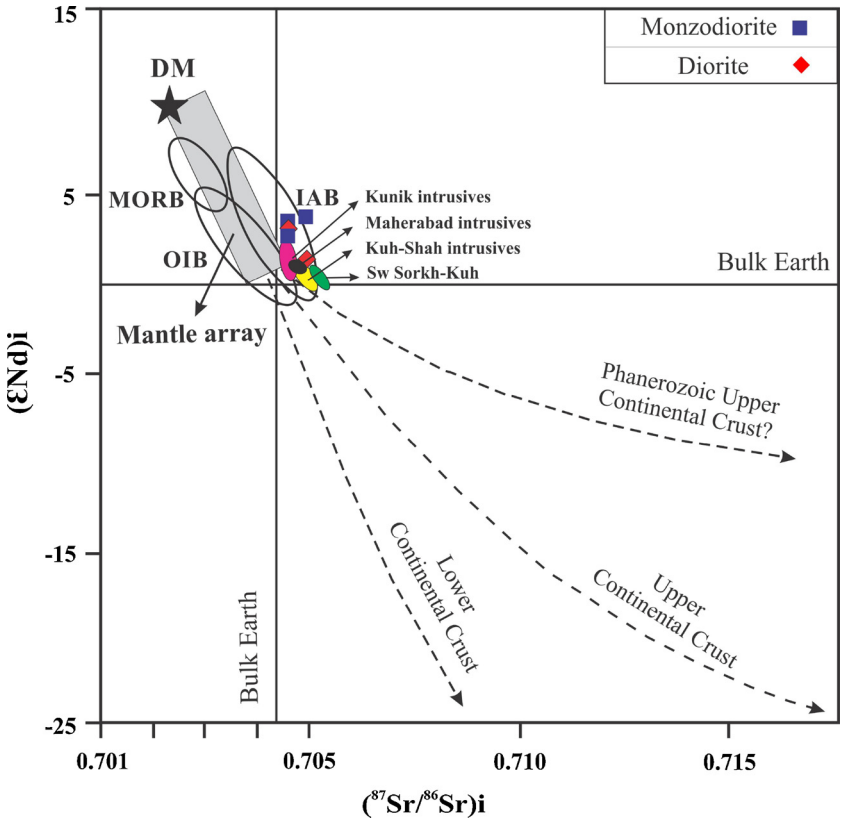

Fig. 7. εNd(i) *vs.* $(^{87}Sr/^{86}Sr)i$ diagram for the SSA rocks. Reference data sources: upper continental crust (Taylor and McLennan, 1985); lower continental crust (Rollinson, 1993; Rudnick, 1995) with those of MORB: Mid-ocean ridge basalts (Rollinson, 1993; Sun and McDonough, 1989), DM: Depleted mantle (McCulloch and Bennett, 1994), OIB: Ocean-island basalts (Vervoort et al., 1999) and mantle array (Wilson, 1989; Gill, 1981). Data for Maherabad and Khopik granitoid rocks from Malekzadeh Shafaroudi et al., (2010); Kuh-Shah from Abdi and Karimpour, 2013; Khunik from Samiee et al., (2016) and SW Sorkh-Kuh intrusive rocks from Hosseinkhani et al., (2017).

Table 4
Rb-Sr and Sm-Nd isotopic data of intrusive rocks in the neighborhood of SSA area (1 = Malekzadeh Shafaroudi et al. (2010); 2 = Abdi and Karimpour (2013); 3 = Samiee et al. (2016); 4 = Hosseinkhani et al. (2017).

Rb-Sr and Sm-Nd isotopic data

Sample	$(^{87}Sr/^{86}Sr)i$	$(^{143}Nd/^{144}Nd)i$	(εNd)i	U-Pb (Ma)
Maherabad and Khopik [1]	0.704756–0.704869	0.512694–0.512713	1.45–1.81	39 Ma
Kuh-Shah [2]	0.704992–0.705191	0.512608–0.512674	−0.18–1.09	39.6 Ma
Khunik [3]	0.704196–0.704772	0.512690–0.512793	1.3–3.3	38 Ma
SW Sorkh-Kuh [4]	0.705521–0.706631	0.512595–0.512727	−0.33–1.88	20 Ma and 40 Ma

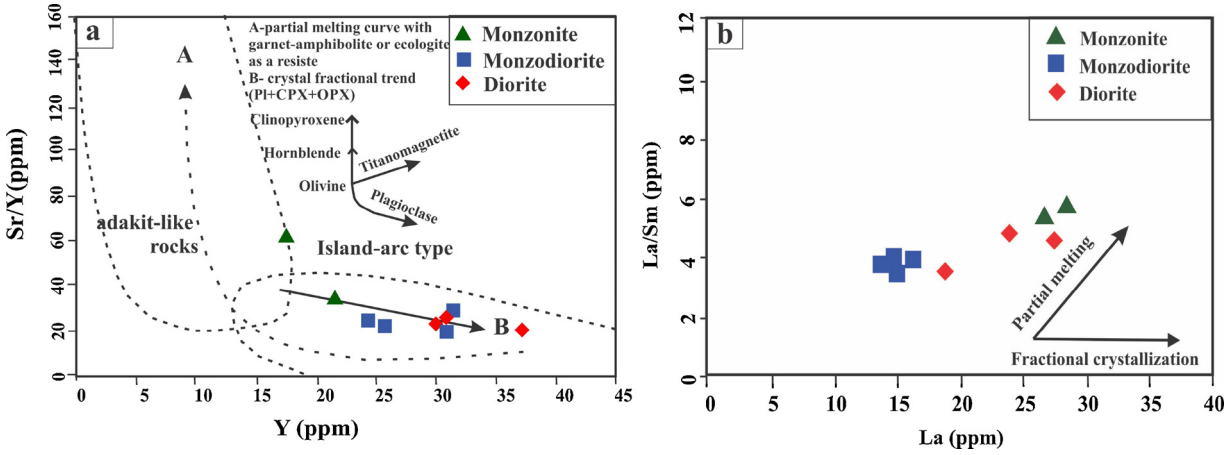

Fig. 8. Diagrams of Sr/Y vs. Y (from Defant and Drummond, 1990), black arrow trend indicate the presence of hornblende, clinopyroxene, titanomagnetite and plagioclase in the source (after Castillo, 2012) (a). La/Sm vs. La (ppm) diagram (Blein et al., 2001) for the SSA subvolcanic porphyries (b).

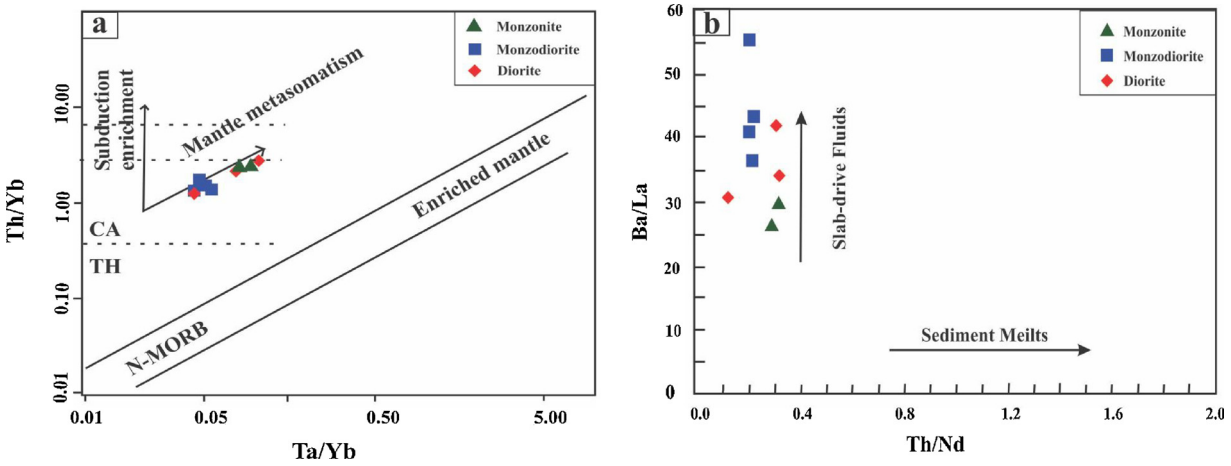

Fig. 9. Th/Yb vs. Ta/Yb diagram (Pearce, 1983) for the SSA subvolcanic porphyries (a). Ba/La vs. Th/Nd diagram (Shaw, 1970). All of the samples follow the slab-derived fluid melt array (b).

garnet in the source, we suggest that magma was formed at depths less than 50 Km, because garnet appears at depths greater than 45–50 km.

9.2. Magma evolution

Different variations in magma can be explained by several mechanisms, such as crystal fractionation, partial melting, magma mixing and assimilation. The $(^{87}Sr/^{86}Sr)_i$ ratios in the SSA subvolcanic units vary from 0.7043 to 0.7052. According to Haschke et al. (2010) increases in $(^{87}Sr/^{86}Sr)_i$ ratios generally indicate the involvement of an older, more radiogenic lithospheric mantle, assimilation of more radiogenic crustal or contamination by subduction-related fluids and/or sediments whereas relatively lower Sr isotope ratios generally reflect mantle source affinities. Furthermore, Nabatian et al. (2014) believe

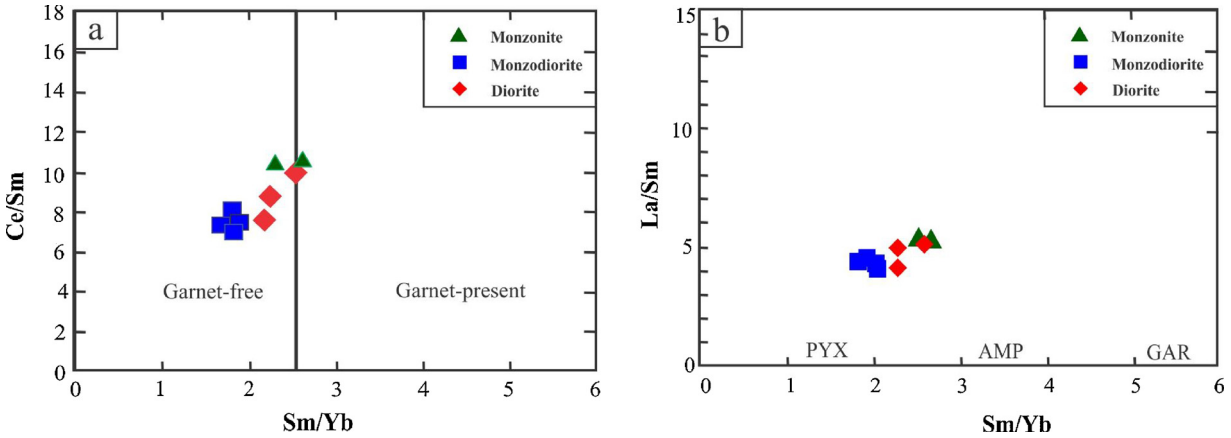

Fig. 10. Ce/Sm vs. Sm/Yb diagram (COBAN, 2007) showing the absence of garnet at source (a). La/Sm vs. Sm/Yb plot showing the fields for the SSA intrusive rocks (b), PYX = pyroxene, AMP = amphobole, GAR = garnet: garnet (modified from Kay and Mpodozis, 2001).

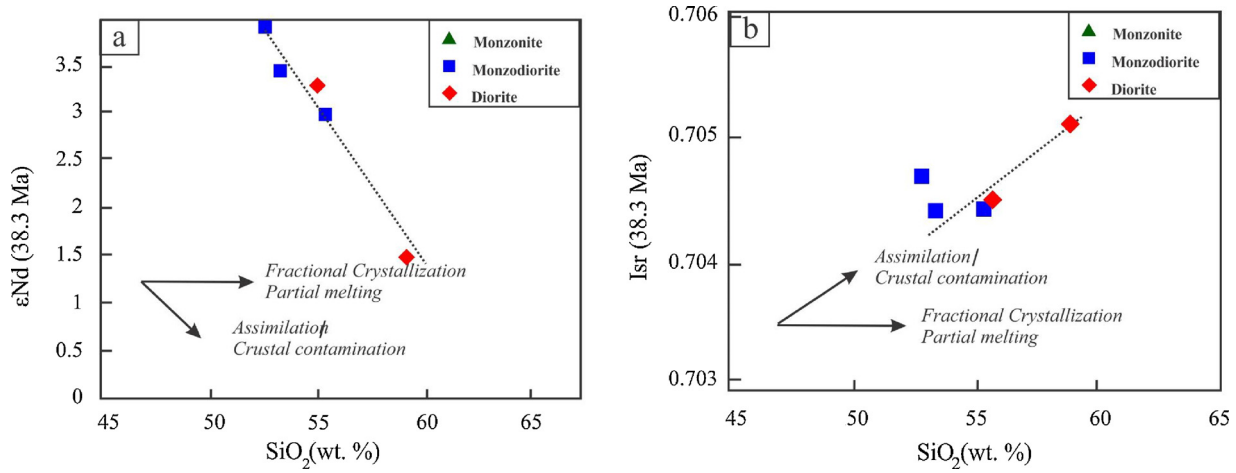

Fig. 11. A plot of (a) εNd vs. SiO_2 (wt. %), (b) ISr vs. SiO_2 (wt. %) of the SSA intrusive rocks. Diagrams plotted according to Maghdour-Mashhour et al. (2015).

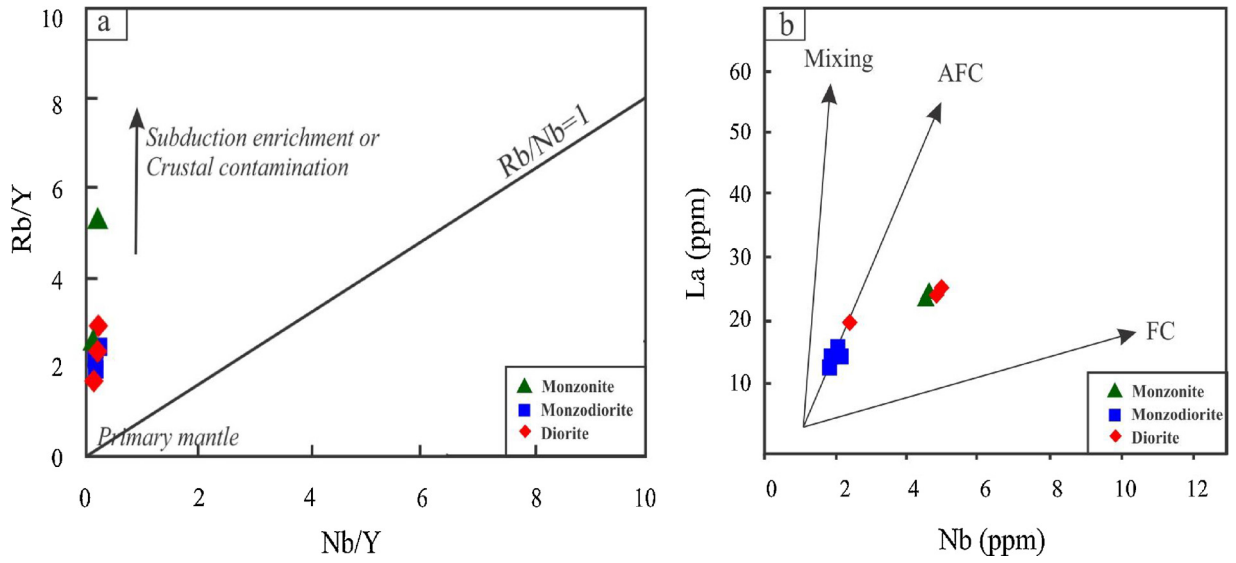

Fig. 12. A plot of Rb/Y versus Nb/Y, showing the roles of subduction enrichment, and crustal contamination in the evolution of the magmas (crustal contamination data from Rudnick and Gao, 2003) (a); Modeling of fractional crystallization (FC), assimilation-fractional crystallization (AFC) and mixing for SSA intrusive rocks in La vs. Nb diagram (b).

that the small variations in isotopic ratios of similar samples can be related either to variable crustal assimilation or to heterogeneity in the magma source. All samples from the SSA area have positive εNd (i) isotope values ranging from +1.48 to +3.81. A plot of εNd against SiO_2 (wt. %) shows negative correlations between SiO_2 content and εNd values (Fig. 11a), whereas ISr (38.3 Ma) ratios of these samples exhibit a positive correlation with SiO_2 (Fig. 11b). In these diagrams, magma mixing or crustal contamination indicate as part of the magma evolution. The role of crustal contamination in the evolution of the magma can be explained by diagram of Rb/Y versus Nb/Y (Fig. 12a). It shows that all samples plot between primary mantle and crustal contamination or subduction enrichment. In the igneous rocks of SSA area, the Ce/Yb ratios vary from 12 to 26 therefore, these low ratios and enrichment in Rb, Cs and K elements can be related to low contamination by crustal materials and low thickness of the crust (Jamali, 2017).

Based on previous studies including moderately light REE (LREE) enrichment, limited range of SiO_2 contents (53.12 to 59.79 wt. %), isotopic data and according to La/Sm vs. La diagram of Blein et al, (2001), it can concluded that sub-volcanic intrusions are co-genetic and deriving from the same parental magma and it formed during partial melting process.

Due to widespread alteration with mineralization in the SSA area, small variations in isotopic ratios can be explained by hydrothermal alteration in this area and role of crustal contamination in magma evolution was not outstanding.

Three important processes such as fractional crystallization (FC), mixing and assimilation and fractional crystallization (AFC) have a significant effect on the composition of the magma that will be produced. To determine the important factor in the formation of SSA rocks La vs. Nb diagram is used (Fig. 12b). The observed trends appear to be consistent with an evolution of the SSA rocks by AFC process. This model is consistent with the observed trends, and this could also be accounted for the discrete trace element patterns.

9.3. Tectonic setting

According to Karimpour et al., (2011), subduction zone existed in the eastern part of Iran (between Lut and Afghan Blocks). The SSA area was affected by the magmatic activity of this subduction zone. Geochemical data show that SSA intrusive rocks in the geotectonic classification of Pearce et al. (1984) are located in volcanic arc granites group. The Rb (53.3–102.2 ppm) and Ta + Yb (1.94–2.39 ppm) values of subvolcanic intrusive units are shown in Rb vs. Ta + Yb diagram of Pearce et al., (1984) (Fig. 13a). By using Zr vs. Y diagram of Müller

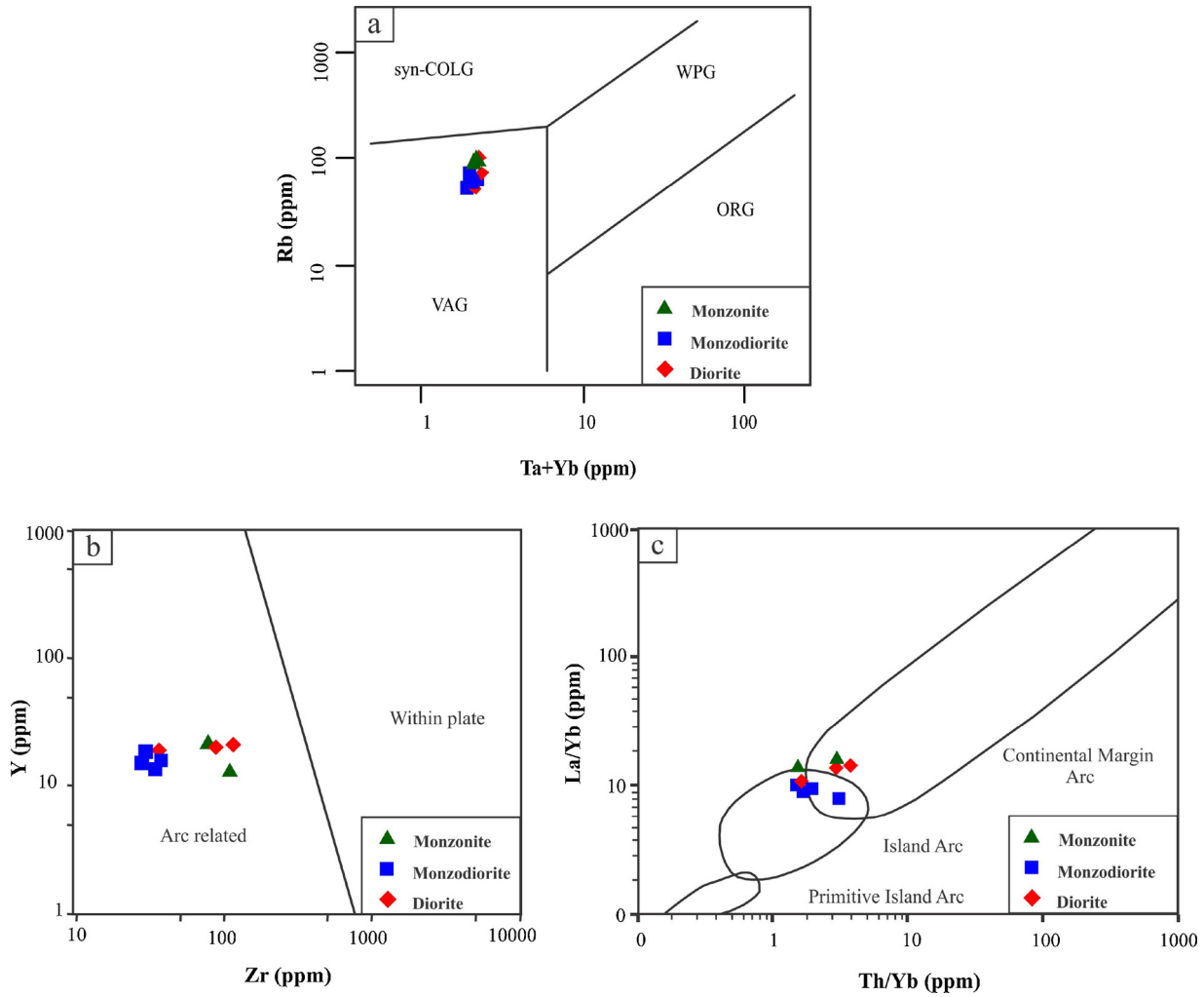

Fig. 13. Tectonomagmatic discrimination diagrams for the SSA intrusive rocks (Pearce et al., 1984). Rb vs. (Ta + Yb) (a). Zr vs. Y diagram (Müller et al., 1994) (b) Th/Yb vs. La/Yb diagram of the SSA intrusive rocks (c) (Brown et al., 1984). WPG: within-plate granitoids; VAG: volcanic arc granitoids; ORG: ocean ridge granitoids; syn-COLG: syncollisional granitoids.

et al. (1994) (Fig. 13b), intrusive rocks fall in arc related field and this shows that magmas are generally ascribed to subduction-related environments. For separation, island arc from continental margin arc used of La/Yb vs. Th/Yb diagram (Brown et al., 1984). In these samples La/Yb and Th/Yb ratios vary from 1.58 to 3.58 and 6.83 to 14.4, respectively. Therefore SSA intrusive rocks were located in the field of continental margin arc and only samples from monzodiorite rocks, shifted toward the island arc field (Fig. 13c). In other words, some samples were plotted in the field of transitional zone between island arc and continental arc (Fig. 13c).

9.4. Tectonic model for the SSA area

As stated, magmatism in the SSA area is related to the subduction zone between Lut and Afghan Blocks. Tectonic setting of volcanic arc, dependence on the oxidant type granitoids (I-type) and negative anomaly of the Ti along with an abundance of mafic minerals altered to Fe-oxide minerals suggest that magma had oxidation state. During the subduction of the Neo- Tethys oceanic slab (Fig. 14), parental magma originated from partial melting of an enriched mantle and it metasomatized by slab-derived fluids that these fluids played an important role in reducing the melting temperature. Eventually, magma ascended into shallow reservoirs in the upper crust and AFC processes were effective in intrusive rocks formation. This model suggests that a minor crustal contamination occurred in the crust. Enrichment in Rb, Cs and K elements show that magma was contaminated by the crustal material. This magma in the source was probably oxidized and enriched in economic elements such as Cu and Au. (Fig. 14).

10. Conclusion

The relationship between magmatism with the subduction zone is very clear in the SSA area. In this area, different types of subvolcanic intrusive units were detected that most of them belonged to Middle-Late Eocene time. Some of the subvolcanic intrusions such as monzonite porphyry and monzodiorite porphyry associated with Cu mineralization. Due to the importance of mineralized subvolcanic intrusions, some characteristics are presented in this paper such as:

1 Based on geochemical data, the subvolcanic intrusive units are metaluminous and belong to I-type granitoids or magnetite-series. These units display high-K calc-alkaline to shoshonitic affinity and are formed in volcanic arc setting at a convergent plate boundary (subduction zone). All the above features are similar to other intrusions which are known in the vicinity of SSA area. Negative anomaly of Nb, enrichment of LILE compared to HFSE elements and tectonic setting (VAG) along with the above features point out are related to subduction environment.
2 Zircon U-Pb dating using LA-ICP-MS indicates that magmatic activity happened during two steps: A. Volcanic activity at 38.9 Ma. B.

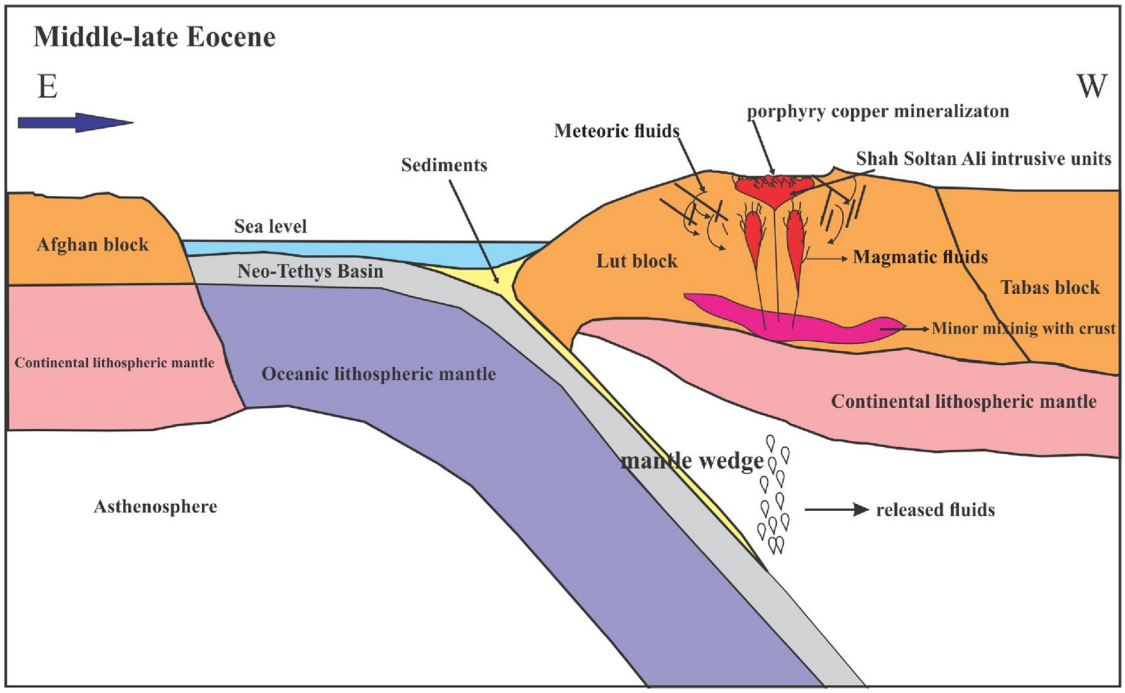

Fig. 14. Simplified geodynamic setting of Lut Block. This model is illustrated as a hypothesis for the tectonomagmatic and mineralization in the SSA area.

Intrusive rocks formed in 38.3 (Bartonian). These results show that the westward subduction of the Neo-Tethys oceanic slab beneath the Lut Block occurred before the Middle-Late Eocene (Bartonian).

3 In the study area, magma originated from the partial melting of the enriched mantle, which metasomatized by fluids derived of subducted continental sediments. Amphibole and pyroxene as the residual minerals are present in source and negative Nb anomaly, positive anomalies of Rb, Cs, Ba and K elements are probably related to the processes of contamination or mixing with crustal materials.

Acknowledgments

This research was supported by Ferdowsi University of Mashhad; Ministry of Sciences, Research and Technology of Iran and it has been implemented in the framework of research project No. 3.36776 (5/03/2015). The authors wish to express their gratitude to all researchers whose data on Lut Block were used in this paper. Also we thank Mrs. Sara Ribeiro (Laboratório de Geologia Isotópica da Universidade de Aveiro) for the TIMS analysis and for the guidance and assistance during sample preparation and Ryan Mathur (Department of Geology, Juniata College, Pensylvania, United States) who did the U-Pb Zircon age dating. Part of this research was supported by Ministry of Sciences, Research and Technology of Iran and the first author thanks them for the financial support sabbatical research in Portugal.

References

Abdi, M., Karimpour, M.H., 2013. Petrochemical characteristics and timing of middle eocene granitic magmatism in Kooh-Shah, Lut Block, eastern Iran. Acta Geol. Sin. 84, 1032–1044. https://doi.org/10.1111/1755-6724.12108.

Ahmadzadeh, G., Jahangiri, A., Lentz, D., Mojtahedi, M., 2010. Petrogenesis of plio-quaternary post-collisional ultrapotassic volcanism in NW of Marand, NW Iran. J. Asian Earth Sci. 39, 37–50.

Allen, M.B., Kheirkhah, M., Neill, I., Emami, M.H., McLeod, C.L., 2013. Generation of arc and within-plate chemical signatures in collision zone magmatism: quaternary lavas from Kurdistan Province, Iran. J. Petrol. 54, 887–911.

Angiboust, S., Agard, P., De Hoog, J.C.M., Omrani, J., Plunder, A., 2013. Insights on deep, accretionary subduction processes from the Sistan ophiolitic "mélange" (Eastern Iran). Lithos 156, 139–158. https://doi.org/10.1016/j.lithos.2012.11.007.

Arjmandzadeh, R., Karimpour, M.H., Mazaheri, S.A., Santos, J.F., Medina, J.M., Homam, S.M., 2011. Sr–Nd isotope geochemistry and petrogenesis of the Chah-Shaljami granitoids (Lut block, eastern Iran). J. Asian Earth Sci. 41, 283–296.

Asran, A.M., Rahman, E.M.A., 2012. The Pan-African calc-alkaline granitoids and the associated mafic microgranular enclaves (MME) around Wadi Abu Zawal area, north Eastern Desert, Egypt. Geology, geochemistry and petrogenesis. J. Biol. Earth Sci. 2 (1), 1–16.

Berberian, M., 1977. Against the rigidity of theLut block. Geol. Min. Surv. Iran 40, 203–227.

Berglund, M., Wieser, M.E., 2011. Isotopic compositions of the elements 2009 (IUPAC Technical Report). Pure Appl. Chem. 83, 397–410. https://doi.org/10.1351/PAC-REP-10-06-02.

Blein, O., Lapierre, H., Schweickert, R.A., 2001. A Permian island-arc with a continental basement: the black dyke formation Nevada, North American cordillera. Chem. Geol. 175, 543–566. https://doi.org/10.1016/S0009-2541(00)00357-0.

Boynton, W.V., 1984. Geochemistry of the rare earth elements: meteorite studies. In: Henderson, P. (Ed.), Rare Earth Element Geochemistry. Elsevier, Amsterdam, pp. 63–114.

Brown, G.C., Thorpe, R.S., Webb, P.C., 1984. The geochemical characteristics of granitoids in contrasting arcs and comments on magma sources. J. Geol. Soc. 141 (3), 413–426. https://doi.org/10.1144/gsjgs.141.3.0413. 413-426.

Camp, V., Griffis, R., 1982. Character, genesis and tectonic setting of igneous rocks in the Sistan suture zone, eastern Iran. Lithos 15, 221–239. https://doi.org/10.1016/0024-4937(82)90014-7.

Castillo, P.R., 2012. Adakite petrogenesis. Lithos 134, 304–316. https://doi.org/10.1016/j.lithos.2011.09.013.

Chang, Z., Vervoort, J.D., McClelland, W.C., Knaak, C., 2006. U-Pb dating of zircon by LA-ICP-MS. Geochem. Geophys. Geosyst. 7 (5), 1–14. https://doi.org/10.1029/2005GC001100.

Cherniak, D.J., Watson, E.B., 2000. Pb diffusion in zircon. Chem. Geol. 172, 5–24. https://doi.org/10.1016/S0009-2541(00)00233-3.

Coban, H., 2007. Basalt magma genesis and fractionation in collision-and extension-related provines: a comparison between eastern, central western Anatolia. Earth Sci. Rev. 80, 219–238.

Defant, M.J., Drummond, M.S., 1990. Derivation of modern arc magma by melting of young subducted lithosphere. Nature 347, 662–665.

DePaolo, D.J., Wasserburg, G.J., 1976. Nd isotopic variations and petrogenetic models. Geophys. Res. Lett. 3, 249–252.

Esmaeily, D., Nedelec, A., Valizadeh, M.V., Moore, F., Cotton, J., 2005. Petrology of the Jurassic Shah-kuh granite (eastern Iran), with reference to tin mineralization. J. Asian Earth Sci. 25, 961–980. https://doi.org/10.1016/j.jseaes.2004.09.003.

Gill, J.B., 1981. Orogenic Andesites and Plate Tectonics, Mineral and Rocks. Springer, Berlin, Heidelberg, New York, pp. 390. https://doi.org/10.1017/S0016756800026911.

Haschke, M., Ahmadian, J., Murata, M., McDonald, I., 2010. Copper mineralization prevented by arc-root delamination during Alpine-Himalayan collision in central Iran. Econ. Geol. 105 (4), 855–865. https://doi.org/10.2113/gsecongeo.105.4.855.

Hosseinkhani, M., Karimpour, M.H., Malekzadeh Shafaroudi, A., Santos, J.F., 2017. U-Pb geochronology and petrogenesis of intrusive rocks: constraints on the mode of genesis and timing of Cu mineralization in SWSK area. J. Geochem. Explor. 177, 11–27. https://doi.org/10.1016/j.gexplo.2017.02.001.

Ishihara, S., 1977. The magnetite-series and ilmenite-series granitic rocks. Min. Geol. 27,

293–305.
Ishihara, S., 1981. The granitoid series and mineralization. Econ. Geol. 75, 458–484.
Jahangiri, A., 2007. Post-collisional Miocene adakitic volcanism in NW Iran: geochemical and geodynamic implications. J. Asian Earth Sci. 30, 433–447.
Jamali, H., 2017. The behavior of rare-earth elements, zirconium and hafnium during magma evolution and their application in determining mineralized magmatic suites in subduction zones: constraints from the Cenozoic belts of Iran. Ore Geol. Rev. 81, 270–279.
Jung, D., Keller, J., Khorasani, R., Chr, Marcks, Baumann, A., Horn, P., 1983. Petrology of the Tertiary Magmatic Activity the Northern Lut Area, East of Iran Vol. 51. Ministry of Mines and Metals, GSI, Geodynamic Project (Geotraverse) in Iran, pp. 285–336.
Karimpour, M.H., Stern, C.R., Malekzadeh Shafaroudi, A., Hidarian, M.R., Mazaheri, A., 2009. Petrochemistry of the reduced, ilmenite-series granitoid intrusion related to the Hired Au-Sn prospect, Eastern Iran. J. Appl. Sci. 9, 226–236.
Karimpour, M.H., Stem, C.R., Farmer, L., Saadat, S., Malekezadeh Shafaroudi, A., 2011. Review of age, Rb-Sr geochemistry and petrogenesis of Jurassic to Quaternary igneous rocks in Lut Block, Eastern Iran. J. Geope 1, 19–36.
Kay, S.M., Mpodozis, C., 2001. Central Andean Ore Deposits Linked to Evolving Shallow Subduction System and Thickening Crust: GSA Today 11. pp. 4–9.
Kheirkhah, M., Allen, M.B., Emami, M., 2009. Quaternary syn-collision magmatism from the Iran/Turkey borderlands. J. Volcanol. Geotherm. Res. 182, 1–12.
Maghdour-Mashhour, R., Esmaeily, D., Tabbakh Shabani, A.A., Chiaradia, M., Latypov, R., 2015. Petrology and geochemistry of the Karaj Dam basement sill: implications for geodynamic evolution of the Alborz magmatic belt. J. Chem. Erde. Geochem. 72, 237–260.
Malekzadeh shafaroudi, A., Karimpour, M.H., Mazaheri, S.A., 2010. Rb–Sr and Sm–Nd isotopic compositions and Petrogenesis of ore-related intrusive rocks of gold-rich porphyry copper Maherabad prospect area (North of Hanich), east of Iran. J. Crystallogr. Mineral. 18 (2), 15–32 (in Persian with English abstract).
Martin, H., 1999. Adakitic magmas: modern analogues of Archaean granitoids. Lithos 46, 411–429. https://doi.org/10.1016/S0024-4937(98)00076-0.
McCulloch, M.T., Bennett, V.C., 1994. Progressive growth of the Earth's continental crust and depleted mantle: geochemical constraints. Acta Geol. Sin. 58, 4717–4738. https://doi.org/10.1016/0016-7037(94)90203-8.
Middlemost, E.A.K., 1985. Magmas and Magmatic Rocks: an Introduction to Igneous Petrology. Longman, London, pp. 221–226.
Mohammadi, A., Burg, J.P., Bouilhol, P., Ruh, J., 2016. U–Pb geochronology and geochemistry of Zahedan and Shah Kuh plutons, southeast Iran: implication for closure of the South Sistan suture zone. Lithos 248, 293–308.
Moradi, M., Karimpour, M.H., Farmer, L.G., Stern, C.R., 2011. Rb-Sr and Sm-Nd isotopic composition, U-Pb-Th (zircon) geochronology and petrogenesis of Najmabad granodiorite batholith. J. Econ. Geol. 2 (3), 127–145 (In Persian with English abstract).
Müller, D., Groves, D.I., Heithersay, P.S., 1994. The shoshonite porphyry Cu-Au association in the Goonumbla district, NSW, Australia. Mineral. Petrol. 51 (2–4), 299–321.
Nabatian, G., Ghaderi, M., Neubauer, F., Honarmand, M., Liu, X., Dong, Y., Jiang, S., Quadt, A., Bernroide, M., 2014. Petrogenesis of Tarom high-potassic granitoids in the Alborz-Azarbaijan belt, Iran: geochemical, U–Pb zircon and Sr–Nd–Pb isotopic constraints. Lithos 184, 324–345. https://doi.org/10.1016/j.lithos.2013.11.002.
Nagudi, B., Koeberl, C., Kurat, G., 2003. Petrography and geochemistry of the Singo granite, Uganda, and implications for its origin. J. Afr. Earth Sci. 36 (1), 73–87. https://doi.org/10.1016/S0899-5362(03)00014-9.
Omrani, J., Agard, P., Whitechurch, H., Benoit, M., Prouteau, G., Jolivet, L., 2008. Arc-magmatism and subduction history beneath the Zagros Mountains, Iran: a new report of adakites and geodynamic consequences. Lithos 106, 380–398.
Pang, K.-N., Chung, S.-L., Zarrinkoub, M.H., Mohammadi, S.S., Yang, H.-M., Chu, C.-H., Lee, H.-Y., Lo, C.-H., 2012. Age, geochemical characteristics and petrogenesis of Late Cenozoic intraplate alkali basalts in the Lut–Sistan region, eastern Iran. Chem. Geol. 306–307, 40–53.
Pang, K.N., Chung, S.L., Zarrinkoub, A.H., Khatib, M.M., Mohammadi, S.S., Chiu, H.Y., Chu, C.H., Lee, H.Y., Lo, C.H., 2013. Eocene–oligocene post-collisional magmatism in the Lut–sistan region, eastern Iran: magma genesis and tectonic implications. Lithos 180–181, 234–251. https://doi.org/10.1016/j.lithos.2013.05.009.
Pearce, J.A., 1983. Role of the sub-continental lithosphere in magma genesis at active continental margins. In: Hawkesworth, C.J., Norry, M.J. (Eds.), Continental Basalts and Mantle Xenoliths. Shiva, Nantwich, pp. 230–249.
Pearce, J.A., Harris, N.W., Tindle, A.G., 1984. Trace element discrimination diagrams for the tectonic interpretation of granitic rocks. J. Petrol. 25, 956–983. https://doi.org/10.1093/petrology/25.4.956.
Peccerillo, A., Taylor, S.R., 1976. Geochemistry of Eocene calc-alkaline volcanic rocks from the Kastamonu area (northern Turkey). Contrib. Mineral. Petrol. 58, 63–81.
Richards, J.P., 2012. Discussion of Sun et al. (2011): the genetic association of adakites and Cu–Au ore deposits. Int. Geol. Rev. 368–369.
Rollinson, H.R., 1993. Using Geochemical Data, Evaluation, Presentation, Interpretation. Pearson Education Asia (Pte) Ltd. Longman Science and Technical, Singapore, pp. 352.
Rudnick, R.L., 1995. Making continental crust. Nature 378, 571–578. https://doi.org/10.1038/378571a0.
Rudnick, R.L., Gao, S., 2003. The composition of the continental crust. In: Rudnick, R.L. (Ed.), The Crust. Elsevier-Pergamon, Oxford, pp. 1–64.
Saadat, S., Stern, C.R., 2014. Petrochemistry of ultrapotassic tephrites and associated cognate plutonic xenoliths from late Quaternary Qa'le Hasan Ali maars, central Iran. J. Asian Earth Sci. 89, 108–122. https://doi.org/10.1016/j.jseaes.2014.03.021.
Saadat, S., Stern, C.R., 2016. Distribution and geochemical variations among paleogene volcanic rocks from the north-central Lut block, eastern Iran. Ir. J. Earth Sci. 8, 1–24.
Saadat, S., Karimpour, M.H., Stern, C.H., 2010. Petrochemical characteristics of Neogene and quaternary alkali olivine basalts from the western margin of the Lut Block, eastern iran. Ir. J. Earth Sci. 2, 87–106.
Saccani, E., Delavari, M., Beccaluva, L., Amini, S., 2010. Petrological and geochemical constraints on the origin of the Nehbandan ophiolitic complex (eastern Iran): implication for the evolution of the Sistan Ocean. Lithos 117, 209–228.
Samiee, S., Karimpour, M.H., Ghaderi, M., Haidarian Shahri, M.R., Kloetzli, O., Santos, J.F., 2016. Petrogenesis of sub-volcanic rocks from the Khunik prospecting area, south of Birjand, Iran: geochemical, Sr–Nd isotopic and U–Pb zircon constraints. J. Asian Earth Sci. 115, 170–182. https://doi.org/10.1016/j.jseaes.2015.09.023.
Shand, S.J., 1949. Eruptive Rocks: Their Genesis, Composition, Classification, and Their Relation to Ore-deposits. Thomas Murby.
Shaw, D.M., 1970. Trace element fractionation during anataxis. Geochim. Cosmochim. Acta 34, 237–243. https://doi.org/10.1016/0016-7037(70)90009-8.
Sheth, H.C., Torres-Alvarado, I.S., Verma, S.P., 2002. What is the" calc-alkaline rock series". Int. Geol. Rev. 44, 686–701. https://doi.org/10.2747/0020-6814.44.8.686.
Stocklin, J., Nabavi, M.H., 1973. Tectonic Map of Iran. Geological Survey of Iran.
Sun, S.S., McDonough, W.F., 1989. Chemical and Isotopic Systematics of Oceanic Basalts: Implications for Mantle Composition and Processes 42. Geological Society of London, Special Publications, pp. 313–345. https://doi.org/10.1144/GSL.SP.1989.042.01.19.
Tarkian, M., Lotfi, M., Baumann, A., 1983. Tectonic, Magmatism and the Formation of Mineral Deposits in the Central Lut, East Iran, Ministry of Mines and Metals 51. Geological Survey of Iran, Geodynamic Project (Geotraverse) in Iran, pp. 357–383.
Taylor, S.R., McLennan, S.M., 1985. The Continental Crust: Its Composition and Evolution. Blackwell, Oxford, pp. 312.
Tirrul, R., Bell, I.R., Griffis, R.J., Camp, V.E., 1983. The Sistan suture zone of eastern Iran. Geol. Soc. Am. Bull. 94, 134–156. https://doi.org/10.1130/0016-7606(1983)94<134:TSSZOE>2.0.CO;2.
Vahdati Daneshmand, F., 1991. Geological Map of Birjand, 1:250,000. Geological survey of Iran, Tehran, Iran.
Vassigh, M., Soheili, H., 1975. Geological Map of Sar- E – Chah- E – Shur, 1:100,000. Geological Survey of Iran, Tehran, Iran.
Vervoort, J.D., Patchett, P.J., Blichert- Toft, J., Albarede, F., 1999. Relationship between Lu–Hf and Sm–Nd isotopic systems in the global sedimentary system. Earth Planet. Sci. Lett. 168, 79–99. https://doi.org/10.1016/S0012-821X(99)00047-3.
Walker, R., Gans, P., Allen, M.B., Jackson, J., Khatib, M., Marsh, N., Zarrinkoub, M., 2009. Late Cenozoic volcanism and rates of active faulting in eastern Iran. Geophys. J. Int. 177, 783–805.
Whitney, D.L., Evans, B.W., 2010. Abbreviations for names of rock-forming minerals. Am. Mineral. 95, 185–187. https://doi.org/10.2138/am.2010.3371.
Wilson, M., 1989. Igneous Petrogenesis: A Global Tectonic Approach. Harper Collins Academic, pp. 466.
Zarrinkoub, M.H., Pang, K.N., Chung, S.L., Khatib, M.M., Mohammadi, S.S., Chiu, H.Y., Lee, H.Y., 2012. Zircon U–Pb age and geochemical constraints on the origin of the Birjand ophiolite, Sistan suture zone, eastern Iran. Lithos 154, 392–405. https://doi.org/10.1016/j.lithos.2012.08.007.
Zhang, H., Zhang, L., Harris, N., Jin, L., Honglin, Y., 2006. U-Pb zircon ages, geochemical and isotopic compositions of granitoids in Songpan-Garze fold belt, eastern Tibetan Plateau: constraints on petrogenesis and tectonic evolution of the basement. Contrib. Mineral. Petrol. 152, 75–88. https://doi.org/10.1016/j.lithos.2007.01.002.